

Variational Bayesian Inference for Multiple Extended Targets or Unresolved Group Targets Tracking

Yuanhao Cheng, Yunhe Cao, *Member, IEEE*, Tat-Soon Yeo, *Life Fellow, IEEE*, Yulin Zhang, Fu Jie

Abstract—In this work, we propose a method for tracking multiple extended targets or unresolvable group targets in a clutter environment. Firstly, based on the Random Matrix Model (RMM), the joint state of the target is modeled as the Gamma Gaussian Inverse Wishart (GGIW) distribution. Considering the uncertainty of measurement origin caused by the clutters, we adopt the idea of probabilistic data association and describe the joint association event as an unknown parameter in the joint prior distribution. Then the Variational Bayesian Inference (VBI) is employed to approximately solve the non-analytical posterior distribution. Furthermore, to ensure the practicability of the proposed method, we further provide two potential lightweight schemes to reduce its computational complexity. One of them is based on clustering, which effectively prunes the joint association events. The other is a simplification of the variational posterior through marginal association probabilities. Finally, the effectiveness of the proposed method is demonstrated by simulation and real data experiments, and we show that the proposed method outperforms current state-of-the-art methods in terms of accuracy and adaptability.

Index Terms—Extended target tracking, unresolved group target tracking, multiple target tracking, random matrix model, variational Bayesian inference.

I. INTRODUCTION

IN contrast to traditional point target tracking, when tracking extended targets or unresolvable group targets, it is typically assumed that the target will generate multiple measurements in each scan, and the tracking approach focuses more on the use of multiple measurements to simultaneously estimate the kinematic state and extended shape of the target [1], [2].

According to the complexity of the silhouette, the extended shape of the target can be divided into simple axially symmetric shapes such as an ellipse or rectangle [3]–[5], star-convex shape [6], [7], or a complex or irregular shape [8]–[11]. Depending on the complexity of the shape, different models can be selected to estimate the extended shape.

Among them, for targets modeled with regular elliptical shapes, the random matrix model (RMM) [12] is the most widely used model. The RMM represents the elliptical extent of the target as a Positive Semi-Definite Matrix (PSDM), and uses the inverse Wishart distribution to describe the statistical information of the PSDM, which can ensure the conjugation of the distribution under the Bayesian framework.

Since the RMM is easy to integrate into the Kalman filter-based approach, it can be combined with traditional multi-target tracking methods such as the Joint Probabilistic Data Association (JPDA) or the Probabilistic Multi-Hypothesis Tracking (PMHT) to achieve Multiple Extended Target Tracking (METT) or Multiple Unresolvable Group Target Tracking (MGTT) [13], [14]. Considering that the measurement rate of the target is uncertain, the gamma distribution is usually used to represent it. The joint state of the target can then be expressed as a Gamma Gaussian Inverse Wishart (GGIW) distribution based on the RMM. This distribution is usually embedded into the RFS-based filters to deal with complex METT or MGTT scenarios, representative methods include the GGIW-Probability Hypothesis Density (PHD) filter [15], and the state-of-the-art GGIW-Poisson Multi-Bernoulli Mixture (PMBM) filter [16] and its approximate implementation [17]. Furthermore, tracker implementations of these filters can be obtained by introducing the trajectory sets [18]–[20].

However, the above methods suffer from inaccurate shape estimation due to two major shortcomings of the RMM. One is that the standard RMM is unable to explicitly estimate the shape parameters of an ellipse (e.g., orientation, axis length, etc.). Existing methods are improved in two ways: On the one hand, by introducing other auxiliary information, for example, [21] uses an evolution matrix to describe the changes of the extended shape, while [22] introduces a virtual measurement model to adaptively adjust the shape estimation. On the other hand, by modeling the shape parameters more finely, e.g., [23] uses the Multiplicative Error Model (MEM) to decouple the shape parameters into orientation and semi-axis length. This decoupled form of the shape parameters is common in some literature [24], [25], and the MEM can achieve accurate tracking of the variable extended shape of the targets. However, the MEM has a low probability of estimation collapse [26], which can lead to inaccuracies in shape estimation. This phenomenon is still not effectively addressed in multi-target tracking applications with the MEM such as [27], [28].

Another shortcoming of the standard RMM is that it relies on ignoring the influence of measurement noise. As a result, the estimated shape is biased by the measured noise covariance. An improved method [29] sacrifices accuracy to introduce measurement noise, but has the problem of optimality. Subsequent research has found that this shortcoming can be overcome using the Variational Bayesian Inference (VBI) [30]. The VBI aims to approximate the exact posterior

Yuanhao Cheng, Yunhe Cao, Yulin Zhang, and Fu Jie are with the National Laboratory of Radar Signal Processing, Xidian University, Xi'an 710071, China.

Tat-Soon Yeo is with the Department of Electrical and Computer Engineering, National University of Singapore, 119077, Singapore.

using variational distributions by minimizing the Kullback-Leibler Divergence (KLD). In addition, the VBI performs well when dealing with over-parameterized models [31] or nonlinear measurement equations [26], [32]–[34].

For multi-target tracking or single-target tracking in clutter, it is common to include the association variables as a part of the parameters to be estimated by the VBI. For example, [35] regards the association variables as the dynamic parameter and combines with the VBI to realize the tracking of a known number of multiple point targets. [36] performs approximate estimation of association variables and realizes single point target tracking with unknown measurement noise based on the VBI. [37] derives a variational Bayesian approximation based on first-order statistical linearization for the association variables, which enables tracking and shape estimation of a single target in clutter. [38] uses the VBI and the message passing algorithm to achieve a partly resolvable group target tracking, which is essentially the tracking of multiple point targets.

However, the above methods either lack modeling of the target shape or do not consider joint data association for multi-target tracking. So, they are not capable of handling METT or MGTT. In [39] and [40], the VBI is used to implement target tracking modeled with a multi-ellipsoidal shape and considers the association between the measurement and multiple sub-targets. This may seem to meet the need for METT or MGTT, but because of the lack of prior knowledge of the number of measurements, this type of approach also cannot be used directly. In short, there are no examples of the VBI being applied to METT or MGTT.

Therefore, in this work, we propose a novel method for METT or MGTT. The method is based on the RMM and defines the GGIW prior for the target's joint state. To deal with the shortcomings of the standard RMM mentioned above, we first introduce an evolutionary model for the extended shape, and then derive the multi-target approximate posterior with the VBI. This enables our method to take advantages of both RMM and VBI, and be suitable for METT or MGTT applications.

This work helps to inspire the extension of the VBI applications on METT or MGTT, and the main contributions of this work are:

- We propose an RMM-based multi-target tracking method. The method can track multiple extended targets or unresolvable group targets in a cluttered environment with unknown measurement rate and association variables.
- The proposed method incorporates a shape evolution model based on the RMM to obtain a more accurate target shape estimation.
- We combined the concept of JPDA and regarded the multi-target joint data association as the static parameter, and then the well-known VBI is employed to approximate the unanalyzable joint posterior distribution to obtain an estimation of the kinematic state, the extended shape, and the measurement rate of each target.
- To reduce the computational complexity associated with enumerating all possible joint association events, we give two feasible lightweight schemes to improve the utility

of our method: one is based on gating and clustering, and the other is based on marginal association probabilities. These two schemes provide balance between computational complexity and estimation accuracies while still retaining the essential advantages of the proposed method and applications.

This paper is organized as follows. In Section II, the target is modeled by the RMM and we parameterize its joint state. It then introduces the concept of multi-target association events. In the following Section III and Section IV, we discuss our approach based on the Bayesian framework in terms of two parts, i.e., the time update and the measurement update. The VBI of the multi-target posterior distribution, as outlined in Section IV, represents a key area of interest. In Section V, we present two feasible lightweight schemes to reduce the computational complexity of the proposed method, then the comparative experimental results with numerical simulations are given in Section VI. Finally, we draw a conclusion in Section VII.

Remark 1: In general, the extended target and the unresolvable group target are subject to the same notion of tracking, and thus the METT and the MGTT have the same meaning. Consequently, we do not differentiate between these two types of targets in detail, as our approach is applicable to both of them. In what follows, the term “target” will be used to refer to both types of targets for convenience.

II. PROBLEM FORMULATION

A. Modeling with the Random Matrix Model

Consider a n_d -dimensional scenario, the RMM models the shape of a target as an ellipse. At time k , the kinematic state of the target can be expressed as $\mathbf{x}_k \in \mathbb{R}^{n_d \times n_s}$, which contains the states of position, velocity, etc., and n_s is the dimension of the kinematic state in a one-dimensional physical space. Meanwhile, the elliptical shape of the target can be described as a PSDM.

The dynamic model of the target's kinematic state can be expressed as:

$$\mathbf{x}_k = \mathcal{F}_k(\mathbf{x}_{k-1}) + \boldsymbol{\varepsilon}_k \quad (1)$$

where the state transition function $\mathcal{F}(\cdot)$ is used to describe the motion law of the target between adjacent moments. $\boldsymbol{\varepsilon}_k$ denotes the process noise, which is usually modeled as Gaussian white noise $\boldsymbol{\varepsilon}_k \sim \mathcal{N}(0, \mathbf{G}_k)$ and $\mathbf{G}_k \in \mathbb{R}^{n_d n_s \times n_d n_s}$ is the covariance of the process noise. When the motion of the target satisfies linear dynamics, this dynamic model can be simplified as:

$$\mathbf{x}_k = \boldsymbol{\Phi}_k \cdot \mathbf{x}_{k-1} + \boldsymbol{\varepsilon}_k \quad (2)$$

where the state transition matrix $\boldsymbol{\Phi}_k$ satisfies $\boldsymbol{\Phi}_k = \mathbf{F}_k \otimes \mathbf{I}_{n_d}$, $\mathbf{F}_k \in \mathbb{R}^{n_d n_s \times n_d n_s}$ is a dynamic matrix in a one-dimensional physical space, \mathbf{I}_{n_d} denotes the n_d -th order identity matrix, and the symbol ‘ \otimes ’ indicates the Kronecker product.

The dynamic model of the extended matrix \mathbf{X}_k can be expressed as:

$$p(\mathbf{X}_k | \mathbf{X}_{k-1}) = \mathcal{W}(\mathbf{X}_k; \tau_k, \mathbf{E}_k \mathbf{X}_{k-1} \mathbf{E}_k^T) \quad (3)$$

where $\mathcal{W}(\cdot; a, \mathbf{C})$ denotes the density function of the Wishart distribution, the scalar a is the degrees of freedom and

$\mathbf{C} \in \mathbb{R}^{n_d \times n_d}$ is the scale matrix. Notice that in Eq.(3) we employ the shape evolution mechanism from Lan's model [21], and $\mathbf{E}_k \in \mathbb{R}^{n_d \times n_d}$ is an invertible evolution that describes the dependence of the extension on the shape characteristics of the target (e.g. orientation or size). The degrees of freedom τ_k are directly related to the randomness of evolution. Noting that when $\mathbf{E}_k = \mathbf{I}_{n_d} / \sqrt{\tau_k}$ and τ_k do not vary with time, Eq.(3) degenerates into an extended evolution of the general RMM in [12].

The measurements received by the sensor at time k can be denoted as a set $\mathcal{Y}_k = \{\mathbf{y}_k^j\}_{j=1}^{m_k}$, m_k is the total number of measurements. The measurement set \mathcal{Y}_k consists of two parts, namely, $\mathcal{Y}_k = \tilde{\mathcal{Y}}_k \cup \check{\mathcal{Y}}_k$. Among them, $\tilde{\mathcal{Y}}_k = \{\tilde{\mathbf{y}}_k^j\}_{j=1}^{\tilde{m}_k}$ denotes the measurements generated by the targets and $\check{\mathcal{Y}}_k = \{\check{\mathbf{y}}_k^j\}_{j=1}^{\check{m}_k}$ indicates the clutter. Apparently, there is $m_k = \tilde{m}_k + \check{m}_k$.

For the j -th measurement \mathbf{y}_k^j in $\tilde{\mathcal{Y}}_k$, its spatial distribution satisfies:

$$\mathbf{y}_k^j = \mathbf{H}_k \mathbf{x}_k + \mathbf{v}_k^j \quad (4)$$

where \mathbf{x}_k refers specifically to the kinematic state of the target that produces the measurement \mathbf{y}_k^j . We assume that each measurement generated by the target is distributed independently and identically.

The prediction distribution of \mathbf{x}_k can be expressed as:

$$p(\mathbf{x}_k | \tilde{\mathcal{Y}}^{k-1}) \approx \mathcal{N}(\bar{\mathbf{x}}_{k|k-1}; \hat{\mathbf{m}}_{k|k-1}, \hat{\mathbf{P}}_{k|k-1}) \quad (5)$$

where $\hat{\mathbf{m}}_{k|k-1}$ and $\hat{\mathbf{P}}_{k|k-1}$ are the mean and covariance of the prediction distribution $p(\mathbf{x}_k | \tilde{\mathcal{Y}}^{k-1})$, respectively. And $\tilde{\mathcal{Y}}^{k-1} = \{\tilde{\mathcal{Y}}_1, \tilde{\mathcal{Y}}_2, \dots, \tilde{\mathcal{Y}}_k\}$ denotes all measurements of the target captured by the sensor before time k .

In Eq.(4), $\mathbf{H}_k = \check{\mathbf{H}}_k \otimes \mathbf{I}_{n_d}$ with $\check{\mathbf{H}}_k \in \mathbb{R}^{1 \times n_s}$ is the measurement matrix in a one-dimensional physical space. The pseudo-measurement noise $\mathbf{v}_k^j \sim \mathcal{N}(0, \mathbf{D}_k \mathbf{X}_k \mathbf{D}_k^T)$ represents the deviation between the measurement \mathbf{y}_k^j and the center position of the target. $\mathbf{D}_k \in \mathbb{R}^{n_d \times n_d}$ is an invertible matrix describing the distortion of the observed extension and satisfies [21]:

$$\mathbf{D}_k = (s\bar{\mathbf{X}}_{k|k-1} + \mathbf{R}_k)^{-1/2} \bar{\mathbf{X}}_{k|k-1}^{-1/2} \quad (6)$$

where \mathbf{R}_k is the covariance of the true measurement noise $\boldsymbol{\gamma}_k \sim \mathcal{N}(0, \mathbf{R}_k)$ and $\bar{\mathbf{X}}_{k|k-1}$ is the prediction of the extended matrix at time k . s is a scalar that describes the effect of \mathbf{X}_k , it can be used to describe different types of targets¹. Note that \mathbf{E}_k and \mathbf{D}_k improve the description of the dynamic evolution of the extended shape, so that it can estimate the extension in size and orientation with more precision.

Then the prediction distribution of the extended matrix \mathbf{X}_k can be assumed to be:

$$p(\mathbf{X}_k | \tilde{\mathcal{Y}}^{k-1}) \approx \mathcal{IW}(\mathbf{X}_k; \hat{\mathbf{v}}_{k|k-1}, \hat{\mathbf{V}}_{k|k-1}) \quad (7)$$

And we have:

$$\bar{\mathbf{X}}_{k|k-1} \triangleq \mathbb{E}(p(\mathbf{X}_k | \tilde{\mathcal{Y}}^{k-1})) = \hat{\mathbf{V}}_{k|k-1} / (\hat{\mathbf{v}}_{k|k-1} - 2n_d - 2) \quad (8)$$

where $\mathcal{IW}(\cdot; \mathbf{v}, \mathbf{V})$ denotes the inverse Wishart distribution.

¹For a target with an elliptical shape, we have $s = 1/4$ [29].

The measurement model in Eq.(4) is used to describe the distribution of measurements in space, where the number of measurements is usually assumed to obey the Poisson distribution with parameter λ_k . In order to satisfy the conjugate of the joint distribution, it can be assumed that the Poisson parameter λ_k follows the gamma distribution $\lambda_k \sim \mathcal{G}(\lambda_k; \alpha_k, \beta_k)$ with the scalar shape parameter α_k and the scalar scale parameter β_k .

For clutter in the environment at time k , we model it using the common homogeneous Poisson point process (PPP), i.e., assuming the clutter is uniformly distributed in the surveillance area and the number of clutters obeys a Poisson distribution with parameter λ_c which is time invariant.

B. The State Parameters for Multiple Targets

Consider multiple targets and the number of targets is n_k . Let the states of all targets form the set $\Xi_k^{1:n_k} = \{\mathbf{x}_k^{1:n_k}, \mathbf{X}_k^{1:n_k}, \boldsymbol{\Lambda}_k^{1:n_k}\} = \{\mathbf{x}_k^{(n)}, \mathbf{X}_k^{(n)}, \lambda_k^{(n)}\}_{n=1}^{n_k}$, where $\mathbf{x}_k^{(n)} = \{\mathbf{x}_k^{(n)}\}_{n=1}^{n_k}$, $\mathbf{X}_k^{1:n_k} = \{\mathbf{X}_k^{(n)}\}_{n=1}^{n_k}$, and $\boldsymbol{\Lambda}_k^{1:n_k} = \{\lambda_k^{(n)}\}_{n=1}^{n_k}$ denote the set consisting of the kinematic states, the extended matrix and the measurement rate of all targets at time k , respectively. Define random variable $\boldsymbol{\xi}_k^{(n)} = \{\mathbf{m}_k^{(n)}, \mathbf{P}_k^{(n)}, \mathbf{v}_k^{(n)}, \mathbf{V}_k^{(n)}, \alpha_k^{(n)}, \beta_k^{(n)}\}$ represents all the state parameters of the n -th target, then the distribution of the joint state can be represented as the form of GGIW distribution:

$$\begin{aligned} \boldsymbol{\xi}_k^{(n)} &\sim \mathcal{GGIW}(\boldsymbol{\xi}_k^{(n)}; \boldsymbol{\xi}_k^{(n)}) \\ &= \mathcal{GGIW}(\boldsymbol{\xi}_k^{(n)}; \mathbf{m}_k^{(n)}, \mathbf{P}_k^{(n)}, \mathbf{v}_k^{(n)}, \mathbf{V}_k^{(n)}, \alpha_k^{(n)}, \beta_k^{(n)}) \\ &= \mathcal{N}(\mathbf{x}_k^{(n)}; \mathbf{m}_k^{(n)}, \mathbf{P}_k^{(n)}) \cdot \mathcal{IW}(\mathbf{X}_k^{(n)}; \mathbf{v}_k^{(n)}, \mathbf{V}_k^{(n)}) \cdot \mathcal{G}(\lambda_k^{(n)}; \alpha_k^{(n)}, \beta_k^{(n)}) \end{aligned} \quad (9)$$

where $\boldsymbol{\xi}_k^{(n)} = \{\mathbf{x}_k^{(n)}, \mathbf{X}_k^{(n)}, \lambda_k^{(n)}\}$, $n = 1, 2, \dots, n_k$ is the joint state of the n -th target.

Remark 2: In Eq.(9) we assume independence between the target's kinematic state and the extent shape, which is not entirely rigorous. This is because the velocity of the target is often coupled to the orientation of the extent shape, but this assumption is necessary to ensure the conjugation of the joint distribution. See Table I for the complete list of the notations.

C. Multi-Target Joint Association Events

Data association for multi-target tracking means that the m_k measurements from the set $\mathcal{Y}_k = \{\mathbf{y}_k^j\}_{j=1}^{m_k}$ at time k are assigned to n_k ($n_k > 1$) targets. Since the "target" described in this paper is capable of generating multiple measurements at the same time, multiple measurements can be associated with the same target. In other words, data association can be formulated as a multi-to-1 mapping problem. We denote a Joint Association Event (JAE) as $\boldsymbol{\theta}$, it is a vector of size $1 \times m_k$ and can be represented as:

$$\boldsymbol{\theta} = [\theta_1, \theta_2, \dots, \theta_{m_k}]_{1 \times m_k} \quad (10)$$

where the mapping $\vartheta: \mathcal{Y}_k \rightarrow \Xi_k$ satisfies:

$$\begin{cases} \vartheta_j = i, & \text{if measurement } \mathbf{y}_k^j \text{ belongs to } i\text{-th target,} \\ \vartheta_j = 0, & \text{if } \mathbf{y}_k^j \text{ is clutter.} \end{cases} \quad (11)$$

TABLE I: NOTATIONS

- Real number field \mathbb{R} ; Positive integer field \mathbb{Z}^+
- Set of real horizontal vector of length n is represented with \mathbb{R}^n .
- Set of real matrices of size $m \times n$ is represented with $\mathbb{R}^{m \times n}$.
- Set of symmetric positive definite and semi-definite matrices of size $n \times n$ is represented with \mathbb{S}_{++}^n and \mathbb{S}_+^n , respectively.
- $\mathcal{N}(\mathbf{x}; \boldsymbol{\mu}, \boldsymbol{\Sigma})$ represents the multivariate Gaussian distribution with mean vector $\boldsymbol{\mu} \in \mathbb{R}^{n_x}$ and covariance matrix $\boldsymbol{\Sigma} \in \mathbb{S}_{++}^{n_x}$.
- $\mathcal{W}(\mathbf{X}; \nu, \mathbf{V})$ denotes the Wishart distribution with degrees of freedom $\nu \in \mathbb{R}$ and semi-definite scale matrix $\mathbf{V} \in \mathbb{S}_+^{n_x}$, and satisfied:

$$\mathcal{W}(\mathbf{X}; \nu, \mathbf{V}) \propto |\mathbf{X}|^{\frac{\nu}{2}} \text{etr}\left(-\frac{1}{2}\mathbf{X}^{-1}\mathbf{V}\right)$$

where $\text{etr}(\cdot) \triangleq e^{\text{tr}(\cdot)}$.

- $\mathcal{IW}(\mathbf{X}; \hat{\nu}, \hat{\mathbf{V}})$ denotes the inverse Wishart distribution with degrees of freedom $\hat{\nu} \in \mathbb{R}$ and semi-definite scale matrix $\hat{\mathbf{V}} \in \mathbb{S}_+^{n_x}$, and satisfied:

$$\mathcal{IW}(\mathbf{X}; \hat{\nu}, \hat{\mathbf{V}}) \propto |\mathbf{X}|^{-\frac{\hat{\nu}}{2}} \text{etr}\left(-\frac{1}{2}\mathbf{X}^{-1}\hat{\mathbf{V}}\right)$$

- $\mathcal{G}(\lambda; a, b)$ denotes the gamma distribution with scalar shape parameter a and scalar scale parameter b , and satisfied:

$$\mathcal{G}(\lambda; a, b) \propto \lambda^{a-1} e^{-b\lambda}$$

where $\Gamma(\cdot)$ denotes the gamma function.

- $|\mathbf{A}|$ denotes the determinant of the matrix \mathbf{A} , same as $\det[\mathbf{A}]$.
- a^T means find the transpose of a .
- $a!$ means calculating the factorial of a .
- \mathbb{E}_p indicates the expectation operator, and subscript ' p ' emphasizes the underlying probability distribution(s).
- $\text{diag}[a_1, a_2, \dots, a_n]$ returns the diagonal matrix whose diagonal elements are a_1, a_2, \dots, a_n .

Then all JAEs at the time k can be represented as a set $\Theta_k^{1:L_k^\theta} = \{\theta_k^l\}_{l=1}^{L_k^\theta}$, where θ_k^l denotes the l -th JAE at the time k and L_k^θ is the total number of JAEs. Suppose that a certain JAE assigns all measurements in the set $\tilde{\mathcal{Y}}_k^{l-(n)} = \{y_k^{\tilde{j}}\}_{\tilde{j}=1}^{\phi_k^{l-(n)}}$ to the n -th target, where $\phi_k^{l-(n)}$ denotes the number of measurements assigned to the n -th target under the JAE θ_k^l . In particular, $\phi_k^{l-(0)}$ represents the number of clutters in the JAE θ_k^l . Then the likelihood of the measurement set $\tilde{\mathcal{Y}}_k^{(n)}$ can be expressed as:

$$p(\tilde{\mathcal{Y}}_k^{(n)} | \theta_k^l, \xi_k^{(n)}) = \prod_{y_k^{\tilde{j}} \in \tilde{\mathcal{Y}}_k^{(n)}} p(y_k^{\tilde{j}} | \xi_k^{(n)}) \quad (12)$$

$$n = 1, 2, \dots, n_k; \tilde{j} = 1, 2, \dots, \phi_k^{l-(n)}$$

where $p(y_k^{\tilde{j}} | \xi_k^{(n)})$ is the likelihood of a single measurement $y_k^{\tilde{j}}$. According to the measurement model in Eq.(4), we have:

$$p(y_k^{\tilde{j}} | \xi_k^{(n)}) = \mathcal{N}(y_k^{\tilde{j}}; \mathbf{H}_k^{(n)} \mathbf{x}_k^{(n)}, \mathbf{D}_k^{(n)} \mathbf{X}_k^{(n)} (\mathbf{D}_k^{(n)})^T) \quad (13)$$

For simplicity, we assume that the measurement model of each target is the same. Therefore, the superscript ' (n) ' of $\mathbf{H}_k^{(n)}$ can be ignored.

Consider the clutter in the scene, given a JAE θ_k^l , the likelihood of the overall measurement set \mathcal{Y}_k can be expressed as:

$$p(\mathcal{Y}_k | \theta_k^l, \Xi_k^{1:n_k}) = (\rho)^{\phi_k^{l-(0)}} \prod_{n=1}^{n_k} \prod_{y_k^{\tilde{j}} \in \tilde{\mathcal{Y}}_k^{l-(n)}} p(y_k^{\tilde{j}} | \xi_k^{(n)}) \quad (14)$$

where ρ denotes the clutter density. Since we assume the Poisson parameter of the clutter λ_c to be a time-invariant constant, and ρ is also time-invariant and satisfies [41]:

$$\rho = \lambda_c / S_V \quad (15)$$

if the volume of the scene S_V is fixed.

Remark 3: Given a JAE θ_k^l , the number of measurements assigned to each target or clutter in relation to that association event is directly known. This means that a valid JAE can uniquely correspond to a set of measurement cardinality, i.e., $\theta_k^l \rightarrow \Pi_k^l = \{\phi_k^{l-(n)}\}_{n=0}^{n_k}$. Here we illustrate the measurement cardinality set Π_k^l with a simple example.

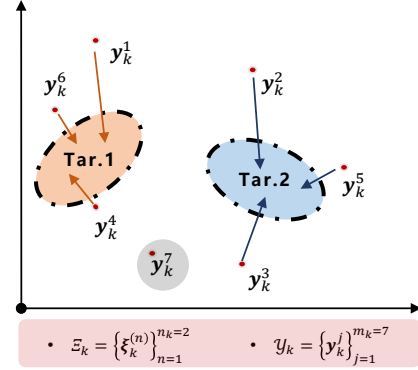


Fig. 1: An example of a valid joint association event.

Example 1: There are $n_k = 2$ targets and $m_k = 7$ unassigned and unknown-origin measurements at the time k . A reasonable JAE is illustrated in Fig.1. In this association event, the measurements $\{y_k^1, y_k^4, y_k^6\}$ are assigned to target 1 (Tar.1), and the measurements $\{y_k^2, y_k^3, y_k^5\}$ are assigned to target 2 (Tar.2), while treating the y_k^7 as clutter. Therefore, according to Eq.(10) and ignore the time subscript ' k ', this JAE can be expressed as $\theta = [1, 2, 2, 1, 2, 1, 0]$, and the corresponding set of measurement cardinality is $\theta \rightarrow \Pi = \{\phi^{(n)}\}_{n=0}^{n=2} = \{\phi^{(0)} = 1, \phi^{(1)} = 3, \phi^{(2)} = 3\}$.

Notice that there is a many-to-1 relationship between the JAE and the cardinality set, i.e., given a cardinality set $\Pi_k = \{\phi_k^{(n)}\}_{n=0}^{n_k}$, the number of JAE it may correspond to is:

$$n_{\text{JAE}} = C_{m_k}^{\phi^{(1)}} C_{m_k - \phi^{(1)}}^{\phi^{(2)}} \cdots C_{m_k - \sum_{n=1}^{n_k-1} \phi_k^{(n)}}^{\phi_k^{(n_k)}} = \frac{m_k!}{\prod_{i=0}^{n_k} \phi_k^{(i)}!} \quad (16)$$

where operation ' C ' represents the calculation of the number of combinations.

Then we can write the conditional probability of the l -th JAE $\theta_k^l, l = 1, \dots, L_k^\theta$ for a multi-target state $\Xi_k^{1:n_k}$ as:

$$p(\theta_k^l | \Xi_k^{1:n_k}) = p(\theta_k^l, \Pi_k^l | \Xi_k^{1:n_k}) \quad (17)$$

$$= p(\theta_k^l | \Xi_k^{1:n_k}, \Pi_k^l) p(\Pi_k^l | \Xi_k^{1:n_k})$$

where Π_k^l is the cardinality set corresponding to the JAE θ_k^l . The last step of Eq.(17) is obtained using the chain rule of conditional probability. For the first term in this step, since the number of measurements generated by the target is assumed to follow a Poisson distribution, there is:

$$p(\theta_k^l | \Xi_k^{1:n_k}, \Pi_k^l) = \prod_{n=0}^{n_k} \mathcal{P}(\phi_k^{l-(n)}; \lambda_k^{(n)}) \quad (18)$$

where the function $\mathcal{P}(\cdot; \lambda)$ represents the Poisson probability density and satisfies $\mathcal{P}(\phi, \lambda) = e^{-\lambda} \frac{\lambda^\phi}{\phi!}$. For the second term $p(\mathbf{\Pi}_k^l | \mathbf{\Xi}_k^{1:n_k})$, because different JAE with equal $\mathbf{\Pi}$ are assumed to be uniformly distributed, we have:

$$p(\mathbf{\Pi}_k^l | \mathbf{\Xi}_k^{1:n_k}) = \frac{1}{n_{\text{JAE}}} = \frac{\prod_{i=0}^{n_k} \phi_k^{l-(n)}!}{m_k!} \quad (19)$$

Substituting Eq.(18) and Eq.(19) into Eq.(17), it can be deduced that:

$$\begin{aligned} p(\theta_k^l | \mathbf{\Xi}_k^{1:n_k}) &= p(\theta_k^l | \mathbf{\Xi}_k^{1:n_k}, \mathbf{\Pi}_k^l) p(\mathbf{\Pi}_k^l | \mathbf{\Xi}_k^{1:n_k}) \\ &= \prod_{n=0}^{n_k} \mathcal{P}(\lambda_k^{(n)}, \phi_k^{l-(n)}) \frac{\prod_{i=0}^{n_k} \phi_k^{l-(n)}!}{m_k!} \\ &= \frac{1}{m_k!} \prod_{n=0}^{n_k} e^{-\lambda_k^{(n)}} \frac{(\lambda_k^{(n)})^{\phi_k^{l-(n)}}}{\phi_k^{l-(n)}!} \cdot \phi_k^{l-(n)}! \\ &= \frac{1}{m_k!} \prod_{n=0}^{n_k} e^{-\lambda_k^{(n)}} (\lambda_k^{(n)})^{\phi_k^{l-(n)}} \end{aligned} \quad (20)$$

According to Bayes rule, the posterior density of the l -th JAE can be calculated as:

$$\begin{aligned} p(\theta_k^l | \mathcal{Y}_k, \mathbf{\Xi}_k^{1:n_k}) &\propto p(\mathcal{Y}_k | \theta_k^l, \mathbf{\Xi}_k^{1:n_k}) p(\theta_k^l | \mathbf{\Xi}_k^{1:n_k}) \\ &\propto \left((\rho)^{\phi_k^{l-(0)}} \prod_{n=1}^{n_k} \prod_{\mathbf{y}_k^j \in \tilde{\mathcal{Y}}_k^{l-(n)}} p(\mathbf{y}_k^j | \xi_k^{(n)}) \right) \left(\frac{1}{m_k!} \prod_{n=0}^{n_k} e^{-\lambda_k^{(n)}} (\lambda_k^{(n)})^{\phi_k^{l-(n)}} \right) \\ &\propto \frac{(\rho)^{\phi_k^{l-(0)}} e^{-\lambda_c} (\lambda_c)^{\phi_k^{l-(0)}}}{m_k!} \prod_{n=1}^{n_k} \left(e^{-\lambda_k^{(n)}} (\lambda_k^{(n)})^{\phi_k^{l-(n)}} \prod_{\mathbf{y}_k^j \in \tilde{\mathcal{Y}}_k^{l-(n)}} p(\mathbf{y}_k^j | \xi_k^{(n)}) \right) \end{aligned} \quad (21)$$

Since the factors $m_k!$ and $e^{-\lambda_c}$ are independent of θ_k^l , so Eq.(21) can be abbreviated as:

$$\begin{aligned} p(\theta_k^l | \mathcal{Y}_k, \mathbf{\Xi}_k^{1:n_k}) &\propto (\rho)^{\phi_k^{l-(0)}} (\lambda_c)^{\phi_k^{l-(0)}} \prod_{n=1}^{n_k} \left(e^{-\lambda_k^{(n)}} (\lambda_k^{(n)})^{\phi_k^{l-(n)}} \prod_{\mathbf{y}_k^j \in \tilde{\mathcal{Y}}_k^{l-(n)}} p(\mathbf{y}_k^j | \xi_k^{(n)}) \right) \end{aligned} \quad (22)$$

We consider the JAE as an unknown parameter, and at the same time an individual JAE has only two cases, occurring or not occurring, which fits the description of the Bernoulli distribution. Thus, the JAE indicator is defined as a Boolean variable $w_k^l, l = 1, 2, \dots, L_k^\theta$. When $w_k^l = 1$ means the l -th JAE occurrence, at this time, for the other JAE, we have $w_k^j = 0$, and w_k^l satisfies $\sum_{l=1}^{L_k^\theta} w_k^l = 1$.

Naturally, the likelihood of the JAE set $\mathbf{\Theta}_k^{1:L_k^\theta}$ can be computed as:

$$\begin{aligned} p(\mathbf{\Theta}_k^{1:L_k^\theta} | \mathcal{Y}_k, \mathbf{\Xi}_k^{1:n_k}) &\propto \prod_{l=1}^{L_k^\theta} [p(\theta_k^l | \mathcal{Y}_k, \mathbf{\Xi}_k^{1:n_k})]^{w_k^l} \\ &= \prod_{l=1}^{L_k^\theta} \left[(\rho)^{\phi_k^{l-(0)}} (\lambda_c)^{\phi_k^{l-(0)}} \prod_{n=1}^{n_k} \left(e^{-\lambda_k^{(n)}} (\lambda_k^{(n)})^{\phi_k^{l-(n)}} \prod_{\mathbf{y}_k^j \in \tilde{\mathcal{Y}}_k^{l-(n)}} p(\mathbf{y}_k^j | \xi_k^{(n)}) \right) \right]^{w_k^l} \end{aligned} \quad (23)$$

Based on Eq.(12), the likelihood of the measurement set \mathcal{Y}_k can be written as:

$$\begin{aligned} p(\mathcal{Y}_k | \mathbf{\Theta}_k^{1:L_k^\theta}, \mathbf{\Xi}_k^{1:n_k}) &= \prod_{l=1}^{L_k^\theta} \left[(\rho)^{\phi_k^{l-(0)}} \prod_{n=1}^{n_k} \prod_{\mathbf{y}_k^j \in \tilde{\mathcal{Y}}_k^{l-(n)}} p(\mathbf{y}_k^j | \xi_k^{(n)}) \right]^{w_k^l} \\ &= \prod_{l=1}^{L_k^\theta} \left[(\rho)^{\phi_k^{l-(0)}} \prod_{n=1}^{n_k} \prod_{\mathbf{y}_k^j \in \tilde{\mathcal{Y}}_k^{l-(n)}} p(\mathbf{y}_k^j; \mathbf{H}_k^{(n)} \mathbf{x}_k^{(n)}, \mathbf{D}_k^{(n)} \mathbf{X}_k^{(n)} (\mathbf{D}_k^{(n)})^T) \right]^{w_k^l} \end{aligned} \quad (24)$$

The term $\prod_{\mathbf{y}_k^j \in \tilde{\mathcal{Y}}_k^{l-(n)}} p(\mathbf{y}_k^j; \mathbf{H}_k^{(n)} \mathbf{x}_k^{(n)}, \mathbf{D}_k^{(n)} \mathbf{X}_k^{(n)} (\mathbf{D}_k^{(n)})^T)$ in Eq.(24) can be rewritten in a more compact form by using the statistical moments of the measurement set $\tilde{\mathcal{Y}}_k^{l-(n)}$, i.e., shown in Eq.(25).

In Eq.(25), $\bar{\mathbf{y}}_k^{l-(n)}$ and $\bar{\mathbf{Y}}_k^{l-(n)}$ are the equivalent measurement and the equivalent spread of the measurements contained in the set $\tilde{\mathcal{Y}}_k^{l-(n)}$, respectively. They can be calculated as:

$$\bar{\mathbf{y}}_k^{l-(n)} = \frac{1}{\phi_k^{l-(n)}} \sum_{\mathbf{y}_k^j \in \tilde{\mathcal{Y}}_k^{l-(n)}} \mathbf{y}_k^j \quad (26a)$$

$$\bar{\mathbf{Y}}_k^{l-(n)} = \sum_{\mathbf{y}_k^j \in \tilde{\mathcal{Y}}_k^{l-(n)}} (\mathbf{y}_k^j - \bar{\mathbf{y}}_k^{l-(n)}) (\mathbf{y}_k^j - \bar{\mathbf{y}}_k^{l-(n)})^T \quad (26b)$$

These equivalent statistical moments $\bar{\mathbf{y}}_k^{l-(n)}$ and $\bar{\mathbf{Y}}_k^{l-(n)}$ are commonly used to approximate the measurement likelihood of the RMM [29], [32]. The loss of information from the approximation inevitably leads to an error. However, the VBI can effectively reduce information loss to make more accurate estimates [30]. In the following, we will illustrate the proposed method in two steps, the time update and the measurement update, based on the iterative structure of the Bayesian framework.

III. TIME UPDATE

Given the joint posterior density at time $k-1$:

$$\begin{aligned} p(\mathbf{\Xi}_{k-1}^{1:n_{k-1}}, \mathbf{\Theta}_{k-1}^{1:L_{k-1}^\theta} | \mathcal{Y}^{k-1}) &= p(\mathbf{\Xi}_{k-1}^{1:n_{k-1}} | \mathcal{Y}^{k-1}) p(\mathbf{\Theta}_{k-1}^{1:L_{k-1}^\theta} | \mathcal{Y}^{k-1}, \mathbf{\Xi}_{k-1}^{1:n_{k-1}}) \end{aligned} \quad (27)$$

$$\prod_{\bar{y}_k^j \in \bar{\mathcal{Y}}_k^{l-(n)}} p\left(\bar{y}_k^j; \mathbf{H}_k^{(n)} \mathbf{x}_k^{(n)}, \mathbf{D}_k^{(n)} \mathbf{X}_k^{(n)} (\mathbf{D}_k^{(n)})^T\right) \propto \mathcal{N}\left(\bar{y}_k^{l-(n)}; \mathbf{H}_k \mathbf{x}_k^{(n)}, \frac{\mathbf{D}_k^{(n)} \mathbf{X}_k^{(n)} (\mathbf{D}_k^{(n)})^T}{\phi_k^{l-(n)}}\right) \mathcal{W}\left(\bar{\mathbf{Y}}_k^{l-(n)}; \phi_k^{l-(n)} - 1, \mathbf{D}_k^{(n)} \mathbf{X}_k^{(n)} (\mathbf{D}_k^{(n)})^T\right) \quad (25)$$

According to the target's parametric model in Eq.(9), the posterior density $p(\Xi_{k-1}^{1:n_{k-1}} | \mathcal{Y}^{k-1})$ can be expanded as:

$$\begin{aligned} & p(\Xi_{k-1}^{1:n_{k-1}} | \mathcal{Y}^{k-1}) \\ &= p(\mathbf{x}_{k-1}^{1:n_{k-1}} | \mathcal{Y}^{k-1}) p(\mathbf{X}_{k-1}^{1:n_{k-1}} | \mathcal{Y}^{k-1}) p(\Lambda_{k-1}^{1:n_{k-1}} | \mathcal{Y}^{k-1}) \\ &= \prod_{n=1}^{n_{k-1}} \left[\mathcal{N}\left(\mathbf{x}_{k-1}^{(n)}; \hat{\mathbf{m}}_{k-1|k-1}^{(n)}, \hat{\mathbf{P}}_{k-1|k-1}^{(n)}\right) \cdot \mathcal{IW}\left(\mathbf{X}_{k-1}^{(n)}; \hat{\mathbf{v}}_{k-1|k-1}^{(n)}, \hat{\mathbf{V}}_{k-1|k-1}^{(n)}\right) \right. \\ & \quad \left. \cdot \mathcal{G}\left(\lambda_{k-1}^{(n)}; \hat{\alpha}_{k-1|k-1}^{(n)}, \hat{\beta}_{k-1|k-1}^{(n)}\right) \right] \quad (28) \end{aligned}$$

The n -th component in Eq.(28) represents the posterior density of the n -th target at time $k-1$.

For simplicity, the kinematic state of the target is assumed to follow linear dynamics. The predicted density $p(\mathbf{x}_k^{(n)} | \mathcal{Y}^{k-1})$ of the n -th target's kinematic state $\mathbf{x}_k^{(n)}, n = 1, 2, \dots, n_{k-1}$ can be computed using standard Kalman time update:

$$p(\mathbf{x}_k^{(n)} | \mathcal{Y}^{k-1}) \sim \mathcal{N}\left(\mathbf{x}_k^{(n)}; \hat{\mathbf{m}}_{k|k-1}^{(n)}, \hat{\mathbf{P}}_{k|k-1}^{(n)}\right) \quad (29)$$

with

$$\hat{\mathbf{m}}_{k|k-1}^{(n)} = \Phi_k \cdot \hat{\mathbf{m}}_{k-1|k-1}^{(n)} \quad (29a)$$

$$\hat{\mathbf{P}}_{k|k-1}^{(n)} = \Phi_k \hat{\mathbf{P}}_{k-1|k-1}^{(n)} \Phi_k^T + \mathbf{Q}_k \quad (29b)$$

where $\hat{\mathbf{m}}_{k|k-1}^{(n)}$ is the mean predicted density and $\hat{\mathbf{P}}_{k|k-1}^{(n)}$ is the corresponding covariance.

For the extended matrix $\mathbf{X}_k^{(n)}, n = 1, 2, \dots, n_{k-1}$ of the n -th target, we inherit the time update from [21], i.e., the predicted density $p(\mathbf{X}_k^{(n)} | \mathcal{Y}^{k-1})$ obeys:

$$p(\mathbf{X}_k^{(n)} | \mathcal{Y}^{k-1}) \sim \mathcal{N}\left(\mathbf{X}_k^{(n)}; \hat{\mathbf{v}}_{k|k-1}^{(n)}, \hat{\mathbf{V}}_{k|k-1}^{(n)}\right) \quad (30)$$

with

$$\hat{\mathbf{v}}_{k|k-1}^{(n)} = \frac{2\tau_k^{(n)}(\gamma_{k-1}^{(n)} + 1)(\gamma_{k-1}^{(n)} - 1)(\gamma_{k-1}^{(n)} - 2)}{(\gamma_{k-1}^{(n)})^2(\gamma_{k-1}^{(n)} + \tau_k^{(n)})} + 2n_d + 4 \quad (30a)$$

$$\hat{\mathbf{V}}_{k|k-1}^{(n)} = \frac{\tau_k^{(n)}}{\gamma_{k-1}^{(n)}} (\hat{\mathbf{v}}_{k|k-1}^{(n)} - 2n_d - 2) \mathbf{E}_k^{(n)} \hat{\mathbf{V}}_{k-1|k-1}^{(n)} (\mathbf{E}_k^{(n)})^T \quad (30b)$$

$$\gamma_{k-1}^{(n)} = \hat{\mathbf{v}}_{k-1|k-1}^{(n)} - 2n_d - 2 \quad (30c)$$

For the n -th target's measurement rate $\lambda_{k-1}^{(n)}, n = 1, 2, \dots, n_{k-1}$, we employ the forgetting factor $\iota_{k-1}^{(n)} \in \mathbb{R}, \iota_{k-1}^{(n)} > 1$ to describe the change in the measurement rate over time, i.e.,

$$p(\lambda_k^{(n)} | \mathcal{Z}^{k-1}) \sim \mathcal{N}\left(\lambda_k^{(n)}; \hat{\alpha}_{k|k-1}^{(n)}, \hat{\beta}_{k|k-1}^{(n)}\right) \quad (31)$$

with

$$\hat{\alpha}_{k|k-1}^{(n)} = \hat{\alpha}_{k-1|k-1}^{(n)} / \iota_{k-1}^{(n)} \quad (31a)$$

$$\hat{\beta}_{k|k-1}^{(n)} = \hat{\beta}_{k-1|k-1}^{(n)} / \iota_{k-1}^{(n)} \quad (31b)$$

In general, we assume that the pattern of change in the measurement rate is the same for each target and thus can be ignored the superscript ' n ' in $\iota_{k-1}^{(n)}$.

For the posterior density of the JAE set $p(\Theta_{k-1}^{1:L_k^\theta} | \mathcal{Y}^{k-1}, \Xi_{k-1}^{1:n_{k-1}})$ at time $k-1$, it can be naturally transformed into a predictive density by replacing the state parameters with predicted values, so the joint predictive density can be expressed as:

$$\begin{aligned} & p(\Xi_k^{1:n_k}, \Theta_k^{1:L_k^\theta} | \mathcal{Y}^{k-1}) \\ &= p(\Xi_k^{1:n_k} | \mathcal{Y}^{k-1}) p(\Theta_k^{1:L_k^\theta} | \mathcal{Y}^{k-1}, \Xi_k^{1:n_k}) \\ &= \prod_{n=1}^{n_{k-1}} \left[\mathcal{N}\left(\mathbf{x}_{k-1}^{(n)}; \hat{\mathbf{m}}_{k|k-1}^{(n)}, \hat{\mathbf{P}}_{k|k-1}^{(n)}\right) \cdot \mathcal{IW}\left(\mathbf{X}_{k-1}^{(n)}; \hat{\mathbf{v}}_{k|k-1}^{(n)}, \hat{\mathbf{V}}_{k|k-1}^{(n)}\right) \right. \\ & \quad \left. \cdot \mathcal{G}\left(\lambda_{k-1}^{(n)}; \hat{\alpha}_{k|k-1}^{(n)}, \hat{\beta}_{k|k-1}^{(n)}\right) \right] \\ & \quad \times p(\Theta_k^{1:L_k^\theta} | \mathcal{Y}^{k-1}, \Xi_k^{1:n_k}) \quad (32) \end{aligned}$$

IV. MEASUREMENT UPDATE

Since the state parameters of the target are modeled with the GGIW distribution, the joint posterior density $p(\Xi_k^{1:n_k}, \Theta_k^{1:L_k^\theta} | \mathcal{Y}^k)$ contains a total of $6 \cdot n_k$ unknown state parameters. The solution of the exact posterior density is extremely complex, considering that the JAE is also unknown.

The VBI uses multiple variational posterior densities to approximate the true posterior density and iteratively estimates each variational posterior density through the mechanism of Coordinate Ascent Variational Inference (CAVI). Since we employ VBI, it can provide more accurate predictive likelihood estimation, which helps to overcome the impact of ignoring measurement noise on the RMM.

Specifically, the joint posterior density $p(\Xi_k^{1:n_k}, \Theta_k^{1:L_k^\theta} | \mathcal{Y}^k)$ can be decomposed into a product of several variational posterior densities as follows:

$$\begin{aligned} p(\Xi_k^{1:n_k}, \Theta_k^{1:L_k^\theta} | \mathcal{Y}^k) &= p(\mathbf{x}_k^{1:n_k}, \mathbf{X}_k^{1:n_k}, \Lambda_k^{1:n_k}, \Theta_k^{1:L_k^\theta} | \mathcal{Y}^k) \\ &\approx q_{\mathbf{x}}(\mathbf{x}_k^{1:n_k}) q_{\mathbf{X}}(\mathbf{X}_k^{1:n_k}) q_{\Lambda}(\Lambda_k^{1:n_k}) q_{\Theta}(\Theta_k^{1:L_k^\theta}) \quad (33) \end{aligned}$$

where the variational posterior density $q_{*}(\mathbf{x}_k^{1:n_k}) = \prod_{n=1}^{n_k} q_{*}^{(n)}(\mathbf{x}_k^{(n)})$, and ' $*$ ' is the corresponding state. As an example, if ' $*$ ' denotes the kinematic state \mathbf{x} , then we have $q_{\mathbf{x}}(\mathbf{x}_k^{1:n_k}) = \prod_{n=1}^{n_k} q_{\mathbf{x}}^{(n)}(\mathbf{x}_k^{(n)})$.

The purpose of CAVI is to find estimates of unknown parameters in each iteration to minimize the KL divergence between the variational posterior density and the true posterior density. This avoids calculating the exact posterior and the KL divergence between two distributions can be defined as:

$$\mathcal{KL}(q(y) \| p(y)) = \int q(y) \ln \frac{q(y)}{p(y)} dy \quad (34)$$

$$q_{\Theta}(\Theta_k^{1:L_k^\theta}) \propto \prod_{l=1}^{L_k^\theta} \left[(\rho)^{\phi_k^{l-(0)}} (\lambda_c)^{\phi_k^{l-(0)}} \prod_{n=1}^{n_k} \tilde{\mathcal{U}}_{\lambda_k^{(n)}}(\phi_k^{l-(n)}) \prod_{\tilde{\mathbf{y}}_k^j \in \tilde{\mathcal{Y}}_k^{l-(n)}} \mathcal{N}(\tilde{\mathbf{y}}_k^j, \mathbf{H}_k \hat{\mathbf{m}}_{k|k-1}^{(n)}, \mathbf{S}_k^{(n)}) \right]^{w_k^l} \quad (37)$$

Based on the above rules for variational inference, [26] has the following relation:

$$\ln q_{\psi}(\psi_k) \propto \mathbb{E}_{\psi} \left[\ln p(\mathbf{x}_k^{1:n_k}, \mathbf{X}_k^{1:n_k}, \Lambda_k^{1:n_k}, \Theta_k^{1:L_k^\theta}, \mathcal{Y}_k | \mathcal{Y}^{k-1}) \right] + C_{\psi} \quad (35)$$

where $\psi \in \{\mathbf{x}_k^{1:n_k}, \mathbf{X}_k^{1:n_k}, \Lambda_k^{1:n_k}, \Theta_k^{1:L_k^\theta}\}$ and the symbol ‘ ψ ’ represents the set consisting of all unknown parameters except the parameter ψ , e.g., $\mathbb{E}_{\mathbf{x}_k^{(i)}}$ denotes the parameter ‘ $\mathbf{X}_k^{1:n_k}, \Lambda_k^{1:n_k}, \Theta_k^{1:L_k^\theta}$ ’, as well as $\mathbf{x}_k^{(j)}$ in $\mathbf{x}_k^{1:n_k}$, with $i \neq j$. And the term independent of ψ can be absorbed into the constant C_{ψ} .

The joint density $p(\mathbf{x}_k^{1:n_k}, \mathbf{X}_k^{1:n_k}, \Lambda_k^{1:n_k}, \Theta_k^{1:L_k^\theta}, \mathcal{Y}_k | \mathcal{Y}^{k-1})$ in Eq.(35) contains all the information of the posterior density and can be expanded as:

$$\begin{aligned} p(\mathbf{x}_k^{1:n_k}, \mathbf{X}_k^{1:n_k}, \Lambda_k^{1:n_k}, \Theta_k^{1:L_k^\theta}, \mathcal{Y}_k | \mathcal{Y}^{k-1}) \\ = p(\mathcal{Y}_k | \Xi_k^{1:n_k}, \Theta_k^{1:L_k^\theta}) p(\Theta_k^{1:L_k^\theta} | \Xi_k^{1:n_k}, \mathcal{Y}^{k-1}) p(\Xi_k^{1:n_k} | \mathcal{Y}^{k-1}) \end{aligned} \quad (36)$$

where $p(\mathcal{Y}_k | \Xi_k^{1:n_k}, \Theta_k^{1:L_k^\theta})$, $p(\Theta_k^{1:L_k^\theta} | \Xi_k^{1:n_k})$, $p(\Xi_k^{1:n_k} | \mathcal{Y}^{k-1})$ is given in Eq.(24), Eq.(23), and Eq.(32), respectively.

Since the VBI is a process with multiple iterations, here we give the computation of each variational posterior in a single variational Bayesian inference below:

- For the JAE set $\Theta_k^{1:L_k^\theta}$ at time k , its variational posterior density $q_{\Theta}(\Theta_k^{1:L_k^\theta})$ can be calculated as Eq.(37).

In Eq.(37), $\tilde{\mathcal{U}}_{\lambda_k^{(n)}}(\phi_k^{l-(n)}) = \left(\mathbb{E}_{\lambda_k^{(n)}}(\lambda_k^{(n)}) \right)^{\phi_k^{l-(n)}}$, and $\mathbb{E}_{\lambda_k^{(n)}}(\lambda_k^{(n)})$ is the expectation of the n -th target measurement rate, which can be calculated as Eq.(39). In addition, the term $\prod_{\tilde{\mathbf{y}}_k^j \in \tilde{\mathcal{Y}}_k^{(n)}} \mathcal{N}(\tilde{\mathbf{y}}_k^j, \mathbf{H}_k \mathbf{x}_k^{(n)}, \mathbf{S}_k^{(n)})$ is the general likelihood of the measurements generated by the n -th target under the l -th JAE. $\mathbf{S}_k^{(n)}$ is the innovation covariance of the n -th target which can be calculated according to Eq.(45). The proof of Eq.(37) can be found in [42, Appendix A].

Remark 4: The variational posterior $q_{\Theta}(\Theta_k^{1:L_k^\theta})$ in Eq. (37) is rigorously derived by the probabilistic data association, i.e., for each JAE θ_k^l , $l = 1, 2, \dots, L_k^\theta$ in the set $\Theta_k^{1:L_k^\theta}$, the variational posterior can be expressed as the product of the prior and the likelihood. However, since the measurement rate $\lambda_k^{(n)}$, $n = 1, 2, \dots, n_k$ of the target is unknown, we use an expectation $\mathbb{E}_{\lambda_k^{(n)}}(\lambda_k^{(n)})$ instead. This expectation of $\lambda_k^{(n)}$ can be derived by solving for the variational posterior $q_{\Lambda}(\Lambda_k^{1:n_k})$, which demonstrates a typical feature of the VBI.

- For the measurement rate $\lambda_k^{(n)}$, $n = 1, \dots, n_k$ in $\Lambda_k^{1:n_k}$, its variational posterior density $q_{\lambda_k^{(n)}}(\lambda_k^{(n)})$ can be computed as:

$$q_{\lambda_k^{(n)}}(\lambda_k^{(n)}) \sim \mathcal{G}(\lambda_k^{(n)}; \hat{\alpha}_{k|k}^{(n)}, \hat{\beta}_{k|k}^{(n)}) \quad (38)$$

with

$$\hat{\alpha}_{k|k}^{(n)} = \hat{\alpha}_{k|k-1}^{(n)} + \sum_{l=1}^{L_k^\theta} q_{\theta}(w_k^l) \phi_k^{l-(n)} \quad (38a)$$

$$\hat{\beta}_{k|k}^{(n)} = \hat{\beta}_{k|k-1}^{(n)} + \sum_{l=1}^{L_k^\theta} q_{\theta}(w_k^l) \quad (38b)$$

where $q_{\theta}(w_k^l)$ is the value of the variational posterior $q_{\Theta}(\Theta_k)$ taken at $w_k^l = 1$, which corresponds to the JAE θ_k^l . The expectation of the measurement rate of the n -th target $\mathbb{E}_{\lambda_k^{(n)}}(\lambda_k^{(n)})$ can be derived as:

$$\mathbb{E}_{\lambda_k^{(n)}}(\lambda_k^{(n)}) = \frac{\hat{\beta}_{k|k}^{(n)}}{\hat{\alpha}_{k|k}^{(n)}} \quad (39)$$

- For the kinematic state of the target $\mathbf{x}_k^{(n)}$, $n = 1, \dots, n_k$ in $\mathbf{x}_k^{1:n_k}$, its variational posterior density $q_{\mathbf{x}_k^{(n)}}(\mathbf{x}_k^{(n)})$ can be calculated as:

$$q_{\mathbf{x}_k^{(n)}}(\mathbf{x}_k^{(n)}) \sim \mathcal{N}(\mathbf{x}_k^{(n)}; \hat{\mathbf{m}}_{k|k}^{(n)}, \hat{\mathbf{P}}_{k|k}^{(n)}) \quad (40)$$

with

$$\hat{\mathbf{m}}_{k|k}^{(n)} = \hat{\mathbf{m}}_{k|k-1}^{(n)} + \mathbf{K}^{l-(n)} \left(\frac{\sum_{l=1}^{L_k^\theta} q_{\theta}(w_k^l) \phi_k^{l-(n)} \tilde{\mathbf{y}}_k^{l-(n)}}{\sum_{l=1}^{L_k^\theta} q_{\theta}(w_k^l) \phi_k^{l-(n)}} - \mathbf{H}_k \hat{\mathbf{m}}_{k|k-1}^{(n)} \right) \quad (40a)$$

$$\hat{\mathbf{P}}_{k|k}^{(n)} = \hat{\mathbf{P}}_{k|k-1}^{(n)} - \mathbf{K}^{l-(n)} \mathbf{H}_k \hat{\mathbf{m}}_{k|k-1}^{(n)} \quad (40b)$$

$$\mathbf{K}^{l-(n)} = \hat{\mathbf{P}}_{k|k-1}^{(n)} \mathbf{H}_k^T \left(\mathbf{H}_k \hat{\mathbf{P}}_{k|k-1}^{(n)} \mathbf{H}_k^T + \frac{\mathbf{D}_k^{(n)} \mathbb{E}_{\mathbf{X}_k^{(n)}}(\mathbf{X}_k^{(n)}) (\mathbf{D}_k^{(n)})^T}{\sum_{l=1}^{L_k^\theta} q_{\theta}(w_k^l) \phi_k^{l-(n)}} \right)^{-1} \quad (40c)$$

where $\mathbb{E}_{\mathbf{X}_k^{(n)}}(\mathbf{X}_k^{(n)})$ is the expected value of the n -th target's extended matrix, which can be calculated according to Eq.(43).

- For the extended matrix $\mathbf{X}_k^{(n)}$, $n = 1, 2, \dots, n_k$ in $\mathbf{X}_k^{1:n_k}$, its variational posterior density $q_{\mathbf{X}_k^{(n)}}(\mathbf{X}_k^{(n)})$ can be deduced as:

$$q_{\mathbf{X}_k^{(n)}}(\mathbf{X}_k^{(n)}) \sim \mathcal{IW}(\mathbf{X}_k^{(n)}; \hat{\mathbf{v}}_{k|k}^{(n)}, \hat{\mathbf{V}}_{k|k}^{(n)}) \quad (41)$$

with

$$\hat{\mathbf{v}}_{k|k}^{(n)} = \hat{\mathbf{v}}_{k|k-1}^{(n)} + \sum_{l=1}^{L_k^\theta} q_{\theta}(w_k^l) \phi_k^{l-(n)} \quad (41a)$$

$$\hat{\mathbf{V}}_{k|k}^{(n)} = \hat{\mathbf{V}}_{k|k-1}^{(n)} + \sum_{l=1}^{L_k^\theta} q_{\theta}(w_k^l) \mathbf{T}^{l-(n)} \quad (41b)$$

The calculation of the auxiliary variable $\mathbf{T}^{l-(n)}$ is shown in Eq.(42). The expectation $\mathbb{E}_{\mathbf{X}_k^{(n)}}(\mathbf{X}_k^{(n)})$ of the extended matrix $\mathbf{X}_k^{(n)}$ is:

$$\mathbb{E}_{\mathbf{X}_k^{(n)}}(\mathbf{X}_k^{(n)}) = \frac{\hat{\mathbf{V}}_{k|k}^{(n)}}{\hat{\mathbf{v}}_{k|k}^{(n)} - 2n_d - 2} \quad (43)$$

$$\mathbf{T}^{l-(n)} = \left(\mathbf{D}_k^{(n)-1} \left(\bar{\mathbf{y}}_k^{l-(n)} + \phi_k^{l-(n)} (\bar{\mathbf{y}}_k^{l-(n)} - \mathbf{H}_k \hat{\mathbf{m}}_{k|k}^{(n)}) (\bar{\mathbf{y}}_k^{l-(n)} - \mathbf{H}_k \hat{\mathbf{m}}_{k|k}^{(n)})^T + \phi_k^{l-(n)} \mathbf{H}_k \hat{\mathbf{P}}_{k|k}^{(n)} \mathbf{H}_k^T \right) (\mathbf{D}_k^{(n)})^{-T} \right) \quad (42)$$

Algorithm 1: One Cycle of the Proposed Method.

Data: Posterior estimate of state parameters $\{\zeta_{k-1|k-1}^{(n)}\}_{n=1}^{n_{k-1}}$ at time $k-1$.

Result: Posterior estimate of state parameters $\{\zeta_{k|k}^{(n)}\}_{n=1}^{n_k}$ at time k , $n_k = n_{k-1}$.

Time Update:

for $n = 1, 2, \dots, n_k$ **do**

$$\begin{aligned} \hat{\mathbf{m}}_{k|k-1}^{(n)}, \hat{\mathbf{P}}_{k|k-1}^{(n)} &\leftarrow \text{Eq. (29)}, \hat{\mathbf{v}}_{k|k-1}^{(n)}, \hat{\mathbf{V}}_{k|k-1}^{(n)} \leftarrow \text{Eq. (30)} \\ \hat{\alpha}_{k|k-1}^{(n)}, \hat{\beta}_{k|k-1}^{(n)} &\leftarrow \text{Eq. (31)}. \end{aligned}$$

end

Measurement Update:

Initialization:

for $n = 1, 2, \dots, n_k$ **do**

$$\begin{aligned} \hat{\mathbf{m}}_{k|k}^{(n)-[0]} &= \hat{\mathbf{m}}_{k|k-1}^{(n)}, \hat{\mathbf{P}}_{k|k}^{(n)-[0]} = \hat{\mathbf{P}}_{k|k-1}^{(n)}, \hat{\mathbf{v}}_{k|k}^{(n)-[0]} = \hat{\mathbf{v}}_{k|k-1}^{(n)}, \\ \hat{\mathbf{V}}_{k|k}^{(n)-[0]} &= \hat{\mathbf{V}}_{k|k-1}^{(n)}, \hat{\alpha}_{k|k}^{(n)-[0]} = \hat{\alpha}_{k|k-1}^{(n)}, \hat{\beta}_{k|k}^{(n)-[0]} = \hat{\beta}_{k|k-1}^{(n)}. \end{aligned}$$

end

Iterations:

while $t \leq n_{VB}$ **do**

$$q_{\Theta}^{[t]}(\Theta_k^{1:L_k}) \leftarrow \text{Eq. (37)}$$

for $n = 1, 2, \dots, n_k$ **do**

$$\begin{aligned} \hat{\mathbf{m}}_{k|k}^{(n)-[t]}, \hat{\mathbf{P}}_{k|k}^{(n)-[t]} &\leftarrow \text{Eq. (40)}, \hat{\mathbf{v}}_{k|k}^{(n)-[t]}, \hat{\mathbf{V}}_{k|k}^{(n)-[t]} \leftarrow \text{Eq. (41)}, \\ \hat{\alpha}_{k|k}^{(n)-[t]}, \hat{\beta}_{k|k}^{(n)-[t]} &\leftarrow \text{Eq. (38)}, \\ \mathbb{E}_{\lambda_k^{(n)}}^{[t]}(\lambda_k^{(n)}) &\leftarrow \text{Eq. (39)}. \end{aligned}$$

end

end

Posterior Estimate: **for** $n = 1, 2, \dots, n_k$ **do**

$$\begin{aligned} \hat{\mathbf{m}}_{k|k}^{(n)} &= \hat{\mathbf{m}}_{k|k}^{(n)-[n_{VB}]}, \hat{\mathbf{P}}_{k|k}^{(n)} = \hat{\mathbf{P}}_{k|k}^{(n)-[n_{VB}]}, \hat{\mathbf{v}}_{k|k}^{(n)} = \hat{\mathbf{v}}_{k|k}^{(n)-[n_{VB}]}, \\ \hat{\mathbf{V}}_{k|k}^{(n)} &= \hat{\mathbf{V}}_{k|k}^{(n)-[n_{VB}]}, \hat{\alpha}_{k|k}^{(n)} = \hat{\alpha}_{k|k}^{(n)-[n_{VB}]}, \hat{\beta}_{k|k}^{(n)} = \hat{\beta}_{k|k}^{(n)-[n_{VB}]}. \end{aligned}$$

end

The derivation of Eq.(38), Eq.(40), and Eq.(41) are given in [42, Appendix B, C, and D].

Remark 5: For the iterative process of the VBI, the termination of the iteration can usually be decided by monitoring the Evidence Lower BOUND (ELBO). However, for multi-target tracking where real-time performance is required, this step can be practically ignored as the computation of ELBO consumes a lot of resources [35]. As an alternative, we can check convergence by monitoring changes in the statistics of the variational posterior (e.g., the posterior mean of the kinematic state), or the maximum number of iterations n_{VB} can be specified directly [43].

In this study, we terminate the variational iteration by specifying n_{VB} . The pseudo-code of the proposed method in a Bayesian cycle is summarized as Algorithm 1. Note that we use the superscript “ $-[t]$ ” to specify the t -th variational iteration.

V. LIGHTWEIGHT SCHEMES

Notice that the calculation of $q_{\Theta}(w_k^l)$ is performed by enumerating all feasible JAE. In multi-target tracking with n

targets, a feasible JAE implies dividing the measurement set $\mathcal{Y} = \{\mathbf{y}^j\}_{j=1}^m$ containing n measurements into $n+1$ subsets. The total number of partitions for a set with m elements is the result of the m -th Bell number [1] that increases exponentially with increasing m . Therefore, enumerating all the JAE is infeasible while ensuring real-time tracking, and devising a computationally lightweight approach of the proposed method is essential in its application in practical scenarios.

A. Lightweight Scheme I: Gating and Clustering

Based on the property that clutter is sparsely distributed in the surveillance area, the gating technique can be used to remove some of the clutter. By reducing the number of unknown measurements, the total number of feasible JAEs can be pruned. Since the kinematic state of the target is assumed to be a Gaussian distribution, an elliptic gating can be employed. The validation region of the n -target is denoted as:

$$\mathcal{T}_k^{(n)} = \left\{ \mathbf{y}_k^{(n)}; (\mathbf{y}_k^{(n)} - \mathbf{H}_k \hat{\mathbf{m}}_{k|k-1}^{(n)})^T \mathbf{S}_k^{(n)-1} (\mathbf{y}_k^{(n)} - \mathbf{H}_k \hat{\mathbf{m}}_{k|k-1}^{(n)}) \leq \mathbf{g}^2 \right\} \quad (44)$$

where the constant \mathbf{g} is the threshold parameter, and the innovation covariance $\mathbf{S}_k^{(n)}$ for the n -th target can be calculated as:

$$\mathbf{S}_k^{(n)} = \mathbf{H}_k \mathbf{P}_{k|k-1}^{(n)} \mathbf{H}_k^T + \mathbf{D}_k^{(n)} \bar{\mathbf{X}}_{k|k-1}^{(n)} (\mathbf{D}_k^{(n)})^T \quad (45)$$

For an unknown measurement \mathbf{y}_k^j , $j = 1, 2, \dots, m_k$, it is considered valid if it falls within the validation region of any target. Measurements in the measurement set \mathcal{Y} other than valid measurements are rejected as clutter ².

The gating operation relies on a human-specified threshold which cannot exclude all the clutter. There is also a need to partition the remaining valid measurements to obtain multiple JAEs, which is still time-consuming. Fortunately, the measurements of an individual target are clustered in their spatial distribution. Based on this, the clustering methods can be used to further reduce the number of partitioning schemes.

The lightweight scheme combining gating and clustering is widely integrated in multi-target tracking applications [44], [45]. This lightweight processing can reduce the original exponential order complexity to square order. When employing traditional clustering algorithms such as K-Means or density-based spatial clustering, the algorithm exhibits a computational complexity of $O(n_k^2 m_k^2)$ [46].

However, the performance of traditional clustering algorithms is heavily dependent on the prespecified algorithm parameters. This means that when two targets are close to each other, these methods cannot effectively divide the measurements that originate from them into two clusters. Of course, more clustering schemes can be obtained by specifying multiple different algorithm parameters, but it is still problematic as it results in a higher computational cost. Therefore,

²For the RFS-based method, these invalid measurements are still retained and used to judge the newborn targets.

another feasible lightweight scheme is proposed. It is based on the approximation of the posterior density by the marginal association probability between the measurements and the targets without enumeration of measurement partitions.

B. Lightweight Scheme II: Marginal Association Probability

For the measurement \mathbf{y}_k^j , $j = 1, \dots, m_k$ in the measurement set \mathcal{Y}_k at time k . Let $\epsilon_{(n)j}$ represent the marginal association probability that measurement \mathbf{y}_k^j belongs to the n -th target. Then Eq.(38), Eq.(40), and Eq.(41) can be approximated as follows.

The parameters of Gaussian distribution:

$$\hat{\mathbf{m}}_{k|k}^{(n)} \approx \hat{\mathbf{m}}_{k|k}^{*(n)} = \hat{\mathbf{m}}_{k|k-1}^{(n)} + \mathbf{K}^{*(n)} \left(\frac{\sum_{j=1}^{m_k} \epsilon_{(n)j} \mathbf{y}_k^j}{\sum_{j=1}^{m_k} \epsilon_{(n)j}} - \mathbf{H}_k \hat{\mathbf{m}}_{k|k-1}^{(n)} \right) \quad (46a)$$

$$\hat{\mathbf{P}}_{k|k}^{(n)} \approx \hat{\mathbf{P}}_{k|k}^{*(n)} = \hat{\mathbf{P}}_{k|k-1}^{(n)} - \mathbf{K}^{*(n)} \mathbf{H}_k \hat{\mathbf{P}}_{k|k-1}^{(n)} \quad (46b)$$

$$\mathbf{K}^{*(n)} = \hat{\mathbf{P}}_{k|k-1}^{(n)} \mathbf{H}_k^T \left(\mathbf{H}_k \hat{\mathbf{P}}_{k|k-1}^{(n)} \mathbf{H}_k^T + \frac{\mathbf{D}_k^{(n)} \hat{\mathbf{V}}_{k|k}^{*(n)} (\mathbf{D}_k^{(n)})^T}{\sum_{j=1}^{m_k} \epsilon_{(n)j} (\hat{\mathbf{V}}_{k|k}^{*(n)} - 2n_d - 2)} \right)^{-1} \quad (46c)$$

The parameters of inverse Wishart distribution:

$$\hat{\mathbf{v}}_{k|k}^{(n)} \approx \hat{\mathbf{v}}_{k|k}^{*(n)} = \hat{\mathbf{v}}_{k|k-1}^{(n)} + \sum_{j=1}^{m_k} \epsilon_{(n)j} \quad (47a)$$

$$\hat{\mathbf{V}}_{k|k}^{(n)} \approx \hat{\mathbf{V}}_{k|k}^{*(n)} = \hat{\mathbf{V}}_{k|k-1}^{(n)} + \sum_{j=1}^{m_k} \epsilon_{(n)j} \mathbf{U}^{(n)j} \quad (47b)$$

$$\mathbf{U}^{(n)j} = \left(\mathbf{D}_k^{(n)-1} \left((\mathbf{y}_k^j - \mathbf{H}_k \hat{\mathbf{m}}_{k|k}^{(n)}) (\mathbf{y}_k^j - \mathbf{H}_k \hat{\mathbf{m}}_{k|k}^{(n)})^T + \mathbf{H}_k \hat{\mathbf{P}}_{k|k}^{(n)} \mathbf{H}_k^T \right) (\mathbf{D}_k^{(n)})^{-T} \right) \quad (47c)$$

The parameters of gamma distribution:

$$\hat{\alpha}_{k|k}^{(n)} \approx \hat{\alpha}_{k|k}^{*(n)} = \hat{\alpha}_{k|k-1}^{(n)} + \sum_{j=1}^{m_k} \epsilon_{(n)j} \quad (48a)$$

$$\hat{\beta}_{k|k}^{(n)} \approx \hat{\beta}_{k|k}^{*(n)} = \hat{\beta}_{k|k-1}^{(n)} + 1 \quad (48b)$$

where the symbol ‘*’ in the superscript represents an approximation. The marginal probability $\epsilon_{(n)j}$ can be significantly simplified in a similar way as the LMIPDA [47], i.e.,

$$\epsilon_{(n)j} \propto \frac{\mathbb{E}_{\lambda_k^{(n)}} (\lambda_k^{(n)}) \mathcal{L}_{(n)j}}{\left[\sum_{i=1}^{n_k} \mathbb{E}_{\lambda_k^{(i)}} (\lambda_k^{(i)}) \mathcal{L}_{(i)j} \right] + \rho \cdot \lambda_c} \quad (49)$$

where $\mathcal{L}_{(n)j} = p(\mathbf{y}_k^j | \xi_k^{(n)})$ is the likelihood of the measurement \mathbf{y}_k^j on the n -th target and ρ is the clutter density presented in Eq.(15). The calculation of $\mathbb{E}_{\lambda_k^{(n)}} (\lambda_k^{(n)})$ can be referred to Eq.(39). In [42, Appendix E], we provide a brief explanation of the feasibility of this lightweight approach in Eq.(46).

It can be seen from Eq.(49) that the calculation of the marginal association probability is linear in the number of objects and linear in the number of measurements. Therefore, after adopting this lightweight strategy, the overall complexity becomes $n_k \cdot \mathcal{O}(n_k m_k) \sim \mathcal{O}(n_k^2 m_k^2)$. Compared to the $\mathcal{O}(n_k^2 m_k^2)$

complexity of the clustering given in Section V-A, it is significantly smaller.

It is no doubt that such a lightweight operation loses information on the number of measurements ϕ assigned to each target under each JAE. The loss of information will lead to some errors in the shape estimation of the target, but this lightweight scheme reduces the original complexity by an order of magnitude, so it is acceptable.

VI. EXPERIMENTAL RESULTS

A. Methods for Comparison

In this section, we compare our method with other state-of-the-art methods in simulation experiments to demonstrate the superior performance of our method. The methods involved in the comparison are:

- MEM-LJPDA: the MEM with Linear-time JPDA (LJPDA) for tracking proposed in [27].
- RM-JPDA: the RMM with traditional JPDA for tracking proposed in [14].
- RM-T-PMB: the RMM with RFS-based PMBM and trajectory set [18], and we adopt the PMB [17] approximation³.
- RM-VB-DBSCAN (proposed method): the RMM with the VBI for tracking, and use the lightweight scheme based on gating and DB-SCAN [48] clustering described in Section V-A.
- RM-VB-Marginal (proposed method): the RMM with the VBI for tracking and use the lightweight scheme based on the marginal association probability given in Section V-B.

B. Metrics

For performance evaluation of targets estimated with an ellipsoidal extent, [49] has shown a reasonable metric named the Gaussian Wasserstein distance (GWD). Define the GWD between two ellipses $\mathcal{Q}_k^1 = \{\mathbf{x}_k^1, \mathbf{X}_k^1\}$ and $\mathcal{Q}_k^2 = \{\mathbf{x}_k^2, \mathbf{X}_k^2\}$ as:

$$d_{GWD}(\mathcal{Q}_k^1, \mathcal{Q}_k^2) = \sqrt{\left\| \mathbf{H}(\mathbf{x}_k^1 - \mathbf{x}_k^2) \right\|^2 + \text{tr} \left(\mathbf{X}_k^1 + \mathbf{X}_k^2 - 2 \sqrt{\left(\sqrt{\mathbf{X}_k^1} \mathbf{X}_k^2 \sqrt{\mathbf{X}_k^1} \right)} \right)} \quad (50)$$

where \mathbf{q}_1 is the actual value of the elliptic parameter and \mathbf{q}_2 is the estimated value of the elliptic parameter obtained using the tracking method. Symbol ‘ \mathbf{x} ’ denotes the kinematic state of the center of the ellipse and symbol ‘ \mathbf{X} ’ represents the extended shape of the ellipse.

Furthermore, to evaluate the performance of the method on the estimation of the center position of the ellipse and the extended shape, we compute the Root-Mean-Square Error (RMSE) of them at the time k , i.e.,

$$\text{RMSE}_{\text{Pos}}(k) = \sqrt{\frac{1}{m_{\text{MC}}} \sum_{s=1}^{m_{\text{MC}}} \left\| \mathbf{H}(\mathbf{x}_k^1 - \mathbf{x}_k^{2,s}) \right\|^2} \quad (51)$$

³MATLAB code can be found in <https://github.com/yuhsuansia>. Thanks to the authors for their contributions.

$$\text{RMSE}_{\text{Ext}}(k) = \sqrt{\frac{1}{m_{\text{MC}}} \sum_{s=1}^{m_{\text{MC}}} \text{tr} [X_k^1 - X_k^{2,s}]^2} \quad (52)$$

where m_{MC} denotes the number of Monte Carlo (MC) runs. $x_k^{2,s}$ and $X_k^{2,s}$ represent the estimated position and extended matrix of a single target at time k of the s -th MC run, respectively. Furthermore, we will calculate the mean and variance of the above RMSE over the time. For the evaluated state ' \star ', the mean and variance of its RMSE over time are defined as:

$$T_{\text{Mean}}(\text{RMSE}_{\star}) = \frac{1}{K} \sum_{k=1}^K \text{RMSE}_{\star}(k) \quad (53)$$

$$T_{\text{Cov}}(\text{RMSE}_{\star}) = \frac{1}{K} \sum_{k=1}^K (\text{RMSE}_{\star}(k) - T_{\text{Mean}}(\text{RMSE}_{\star}))^2 \quad (54)$$

where K is the number of time steps.

C. The Simulation Scenario

Consider a 2D simulation scene of size $[-50\text{m}, 650\text{m}] \times [-320\text{m}, 320\text{m}]$, where the simulation process consists of 60 time steps, with a time interval of $T=1\text{s}$. At the initial time, there are two targets of different sizes. We refer to the two targets as Tar.1 and Tar.2, respectively. After starting the simulation, these two targets gradually approach with the same speed in the period of 1s~30s. Then they cross at the center of the scene at the 30s with the crossing process lasting for 3s, i.e., from 30s to 33s. Thereafter, these two targets gradually move away from each other from 33s to 60s until the end of the simulation. More details about these two targets are shown in Tab. II.

TABLE II: Details of Tar.1 and Tar.2

	Initial position (m)	Velocity (m/s)	Size (m)	Orientation (rad)
Tar.1	[0, -300]	[11, 7.7]	[60, 30]	$-\pi/3$
Tar.2	[0, 300]	[11, -7.7]	[40, 20]	$-\pi/4$

We show the Ground Truth (GT) of each target in the simulation scenario in Fig. 2:

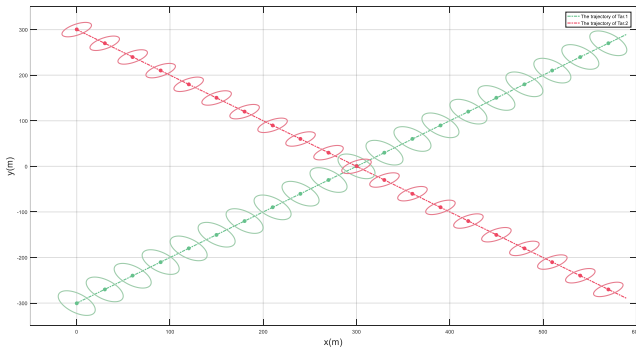


Fig. 2: Ground truth of two targets in the simulation scenario. (The circle shows the extended shape of the targets. We use the green dashed line to mark the trajectory of Tar.1, and the red dashed line to mark the trajectory of Tar.2. The points on the trajectory specify the position of the targets' center)

Other simulation parameters are set as follows:

- Assuming that both targets obey the most common uniform linear motion, the state transition matrix in Eq.(2) is set as:

$$\Phi_k = \begin{bmatrix} 1 & T \\ 0 & 1 \end{bmatrix} \otimes \mathbf{I}_2 \quad \forall k \quad (55)$$

The measurement matrix in Eq.(4) is set as:

$$\mathbf{H}_k = \begin{bmatrix} 1 & 0 & 0 & 1 \\ 0 & 0 & 0 & 0 \end{bmatrix} \quad \forall k \quad (56)$$

The process noise and measurement noise are assumed to be time-invariant and satisfied:

$$\mathbf{G}_k = \text{diag}([1, 1, 0.1, 0.1]); \mathbf{R}_k = \text{diag}([0.01, 0.01]) \quad (57)$$

- Assuming that the clutter obeys a homogeneous PPP with Poisson parameters $\lambda_c = 25$ and is uniformly distributed in the scene. The target generation measure obeys a non-homogeneous PPP, whose measurement rate is assumed to be $\lambda_t = 20$. The detection probability is set as $P_d = 0.98$ that the target is not completely occluded. Of course, the value of λ_t is only used for generating the measurements in simulation, when initializing the measurement rate, we assume that it is unknown and artificially specified as another parameter. The two parameters λ_t and λ_c can be combined as a set of adjustable parameters to simulate different detection situations in the scenario.
- The parameter settings for each method under comparison can be summarized as follows:
 - For all methods, the initial kinematic states of these two targets are set to be consistent, and their measurement rates are assumed to be 80.
 - For MEM-LJPDA, The initial shape states of both targets are set to [orientation, semi-minor axis length, semi-major axis length]=[0rad,20m,20m].
 - For RM-JPDA and RM-T-PMB, set the initial extended matrix of the two targets as $\hat{\mathbf{v}}_{0|0}^{(1)} = \hat{\mathbf{v}}_{0|0}^{(2)} = 7$, $\hat{\mathbf{V}}_{0|0}^{(1)} = \hat{\mathbf{V}}_{0|0}^{(2)} = \text{diag}([400, 400])$. To ensure that the initial extent of targets is the same as MEM-LJPDA.
 - For our methods RM-VB-DBSCAN and RM-VB-Marginal. For the former, the DB-SCAN with different distance thresholds between 0.5 and 10 is applied. For the latter, we set the maximum number of VB iterations to $n_{VB} = 10$. And their parameters of the initialized extended matrix are consistent with RM-JPDA and RM-T-PMB.
 - We perform 100 MC runs on each tracking method⁴.

Fig.3 shows a typical MC run for the simulation scenario with the compared methods (plotted in every 3 time steps). The trajectories and contours of the targets are shown as thicker lines to facilitate comparison. In addition, several representative time-step slices are selected and shown in Fig.7 in an enlarged view. It can be roughly seen from Fig.7 that although each method can effectively track the two targets, there are differences in detail:

⁴All methods are implemented in MATLAB R2016a with Intel (R) Core (TM) i9-10900 CPU and 16 GB RAM.

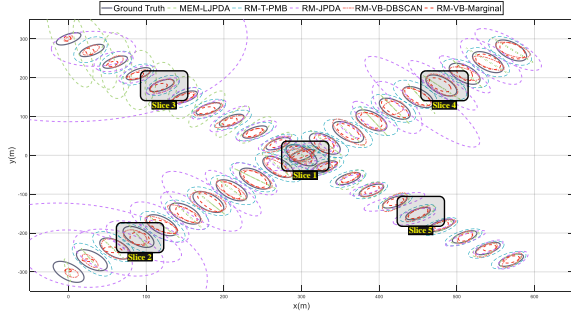


Fig. 3: An example MC run of the simulation scenario.

- For MEM-LJPDA, it suffers from an ‘estimation collapse’ in the shape estimation of Tar.1 (Slice-2 of Fig.7), which results in the collapse of the elliptical contour into a straight line, which is a defect of MEM. Although this phenomenon only occurs in a very limited number of MC runs, it must be emphasized that the effect of this phenomenon on the accuracy of shape estimation is fatal even if it occurs just once. Meanwhile, since MEM-LJPDA lacks the modeling of measurement rate, its convergence to the shape estimation is slower than other methods when the initialized measurement rate is different from the actual measurement rate (Slice-3 of Fig.7).
- For RM-T-PMB and RM-JPDA, their shortcomings seem to be the same, that is, inaccurate estimation of the target shape, since they are based on the original RMM, which captures the change in the shape of the targets by the forgetting factor. Therefore, the accuracy of their shape estimation is highly dependent on the initialization of the extended matrix. As in the simulation, we initialized the shape matrix for RM-T-PMB and RM-JPDA with extended matrices larger and smaller than the real size, respectively. As a result, the shape estimation of RM-T-PMB is larger than the real shape while that of RM-JPDA is smaller.
- Both of our proposed methods, RM-VB-DBSCAN and RM-VB-Marginal, have superior tracking performance. Among them, RM-VB-DBSCAN has the most accurate tracking results because it introduces a shape evolution model and uses the VBI to estimate the state parameters. RM-VB-Marginal is slightly less accurate in shape estimation than RM-VB-DBSCAN, as we analyzed in Section V-B, which is due to neglecting of information about the number of measurements produced by the target.

We plot the acquired metrics, i.e., GWD (averaged over 100 MC runs), $RMSE_{Pos}$, and $RMSE_{Ext}$, in Fig.4, Fig.5 and Fig.6, respectively.

The above metrics further support our conclusions that the MEM-LJPDA converges more slowly (Fig.S3, yellow line). RM-T-PMB and RM-JPDA have large deviations in shape estimation (Fig.6, cyan line and purple line). RM-VB-DBSCAN has the best accuracy in both position estimation and shape estimation (Fig.5 and Fig.6, green line). RM-VB-

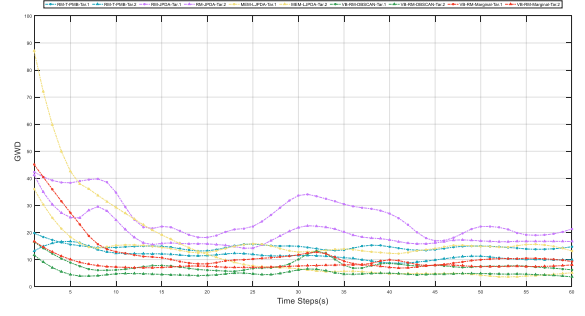


Fig. 4: Simulation results of GWD. (We use different colors to distinguish methods and different markers to distinguish targets. The marker of Tar.1 is ‘•’, and the marker of Tar.2 is ‘▲’)

Marginal has slightly inferior tracking accuracy, this is mainly reflected in the larger bias in shape estimation it has than RM-VB-DBSCAN (Fig.6, red line), but there is no significant difference in the position estimation of the target between these two methods (Fig.5, red line, and green line).

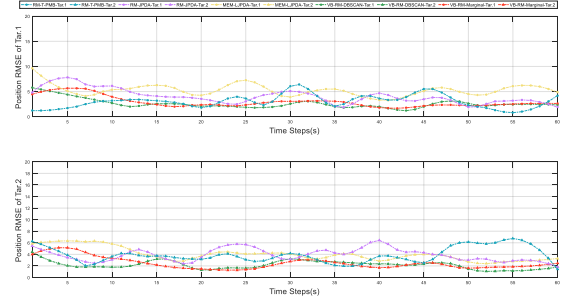


Fig. 5: Simulation results of $RMSE_{Pos}$. (The upper subfigure corresponds to Tar.1, while the lower subfigure corresponds to Tar.2)

In addition, to verify the performance of our proposed method under different measurement conditions, we vary the combinations of parameters (λ_c, λ_t) to construct the following scenarios with different measurement conditions:

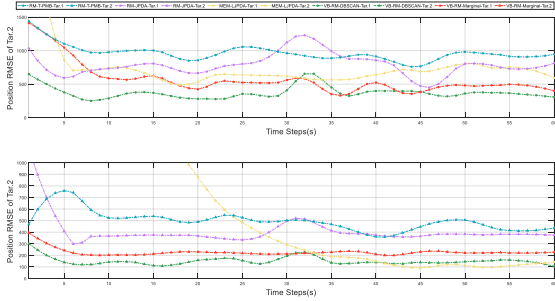
- $(\lambda_c, \lambda_t) = (25, 10)$: There is dense clutter in the scene and the target is detected with few measurements. This combination of parameters is considered the baseline.
- $(\lambda_c, \lambda_t) = (25, 20)$: There is dense clutter in the scene, and the target is able to make more measurements. This combination of parameters is more in line with the actual measurement environment.
- $(\lambda_c, \lambda_t) = (5, 10)$: Sparse clutter in the scene, less measurement of target feedback.
- $(\lambda_c, \lambda_t) = (5, 20)$: Sparse clutter in the scene, and more measurements of the target are captured, this parameter combination meets the ideal detection conditions.

We obtained the statistics of GWD for each tracking method under the above four different combinations of parameters. In addition to $T_{Mean}(RMSE_{Pos})$, $T_{Cov}(RMSE_{Ext})$, and the corresponding covariances are listed in Table III, respectively.

It can be seen from Table III, in terms of both accuracy (Mean.) and stability of the estimate (Var.), the proposed method VB-RM-DBSCAN obtains the best performance in

TABLE III: Statistical information of metrics with different combinations of (λ_c, λ_t)

Methods with parameters (λ_c, λ_t)		GWD [Tar1, Tar2] ↓		RMSE _{Pos} ↓		RMSE _{Ext} ↓	
		Mean.	Var.	Mean.	Var.	Mean.	Var.
MEM-LJPDA	(25,10)	[15.218, 14.775]	[17.367, 309.156]	[5.297, 3.997]	[2.175, 2.038]	[753.231, 1555.341]	[1.943e+05, 1.368e+07]
	(25,20)	[10.716, 7.929]	[61.779, 36.524]	[4.7768, 3.0174]	[1.375, 1.089]	[868.1e+03, 970.2427]	[6.307e+04, 1.765e+03]
	(5,10)	[16.505, 10.622]	[192.918, 95.226]	[5.958, 3.560]	[5.504, 1.339]	[1.857e+03, 1.162e+03]	[9.170e+06, 3.397e+06]
	(5,20) Best PRF.	[5.129, 3.114]	[9.141, 1.964]	[3.712, 2.203]	[0.694, 0.325]	[343.908, 85.823]	[4.960e+05, 5.131e+03]
RM-VB-DBSCAN	(25,10) Best PRF.	[7.954, 4.932]	[7.3180, 2.4351]	[2.584, 2.156]	[1.281, 0.717]	[373.959, 150.218]	[2.0334e+04, 3.1934e+03]
	(25,20) Best PRF.	[5.965, 4.283]	[4.8079, 4.6313]	[2.217, 1.644]	[0.962, 0.539]	[294.944, 145.695]	[1.294e+04, 1.394e+03]
	(5,10) Best PRF.	[7.602, 4.839]	[8.1840, 3.0073]	[3.146, 2.077]	[1.841, 0.637]	[370.502, 159.689]	[2.577e+04, 1.667e+04]
	(5,20)	[5.933, 3.793]	[3.6136, 1.6841]	[2.189, 1.582]	[0.572, 0.248]	[393.357, 121.320]	[1.187e+04, 2.485e+03]
RM-VB-Marginal	(25,10)	[12.741, 7.998]	[63.235, 3.161]	[2.913, 2.470]	[1.271, 1.190]	[593.958, 226.095]	[6.446e+04, 1.148e+03]
	(25,20)	[8.046, 7.782]	[32.838, 2.333]	[2.996, 1.815]	[2.230, 0.464]	[406.932, 229.025]	[1.566e+05, 1.206e+03]
	(5,10)	[8.929, 5.426]	[24.919, 2.705]	[3.232, 2.125]	[2.196, 0.338]	[437.979, 161.454]	[6.307e+04, 1.765e+03]
	(5,20)	[6.567, 4.239]	[15.075, 3.369]	[2.339, 1.646]	[0.698, 0.271]	[325.955, 127.456]	[3.698e+04, 2.253e+03]
RM-T-PMB	(25,10)	[14.686, 11.530]	[1.898, 4.169]	[3.037, 2.962]	[3.882, 2.957]	[953.821, 499.523]	[1.885e+04, 1.004e+04]
	(25,20)	[15.134, 12.330]	[9.593, 5.164]	[3.130, 2.231]	[2.153, 2.498]	[1.013e+03, 566.231]	[7.816e+04, 2.054e+04]
	(5,10)	[15.116, 13.528]	[9.802, 12.094]	[3.190, 2.492]	[2.447, 2.067]	[947.487, 653.663]	[8.017e+04, 4.504e+04]
	(5,20)	[12.544, 10.874]	[1.799, 3.431]	[3.030, 2.051]	[2.603, 2.552]	[649.251, 465.895]	[1.127e+04, 1.077e+04]

Fig. 6: Simulation results of RMSE_{Ext}. (The upper subfigure corresponds to Tar.1, while the lower subfigure corresponds to Tar.2)

the scenarios with the first three parameter combinations (we also mark the "Best performance (Best PRF.))" in this table).

The accuracy of MEM-LJPDA has improved a lot with the reduction of the clutter rate and the increase of the target measurement rate. Under the most ideal observation conditions, i.e., $(\lambda_c, \lambda_t) = (5, 20)$, this method has the best performance. However, such ideal measurement conditions are often not available in practice.

The adaptability to changes in parameter combinations is also demonstrated by another proposed method, RM-VB-Marginal. Moreover, we find that the gap between its accuracy and that of VB-RM-DBSCAN narrows as the clutter decreases (see the metrics of the combinations of parameters $(\lambda_c, \lambda_t) = (5, 20)$ and $(\lambda_c, \lambda_t) = (25, 20)$). This pattern is also reflected in the case of an increase in the target measurement rate (see the metrics of the parameter combinations $(\lambda_c, \lambda_t) = (25, 10)$ and $(\lambda_c, \lambda_t) = (25, 20)$).

We fixed the clutter rate to $\lambda_c = 20$ and adjusted the target measurement rate λ_t from 5 to 30 at intervals of 5.

The average GWD of the two proposed methods are shown in Fig.8. Similarly, we fix the target's measurement rate to $\lambda_t = 20$ and then reduce the Poisson parameter of the clutter λ_c from 20 to 0 in intervals of 5. The variation of the average GWD for the two methods is shown in Fig.9:

Fig.8 and Fig.9 prove that increasing the target measurement rate can narrow the accuracy gap between VB-RM-DBSCAN and RM-VB-Marginal. Meanwhile, reducing the Poisson rate of clutter does not greatly improve the accuracy of VB-RM-DBSCAN, but the improvement of the accuracy of RM-VB-Marginal is significant. The lower clutter rate can quickly reduce the accuracy gap between the two methods. This means that if there is less clutter in the scene, RM-VB-Marginal will be more competitive.

The computational complexity of the tracking methods can be directly judged by the average computational time per MC run, as shown in Table IV. In this table, we use the standard combination of parameters $(\lambda_c, \lambda_t) = (25, 10)$. It can be clearly seen that RM-T-PMB has the highest time cost, because it uses stochastically optimized sampling and considers the case where the number of targets changes. Both RM-VB-DBSCAN and RM-JPDA use the DB-SCAN clustering for lightweight, but the computational time of RM-VB-DBSCAN is slightly higher than that of RM-JPDA because it performs several VBI iterations. Both MEM-LJPDA and RM-VB-Marginal are essentially based on marginal association probabilities for parameter estimation, and thus they have a significant reduction in time cost to linear complexity. However, since RM-VB-Marginal also performs multiple VBI iterations, its complexity is slightly higher than that of MEM-LJPDA.

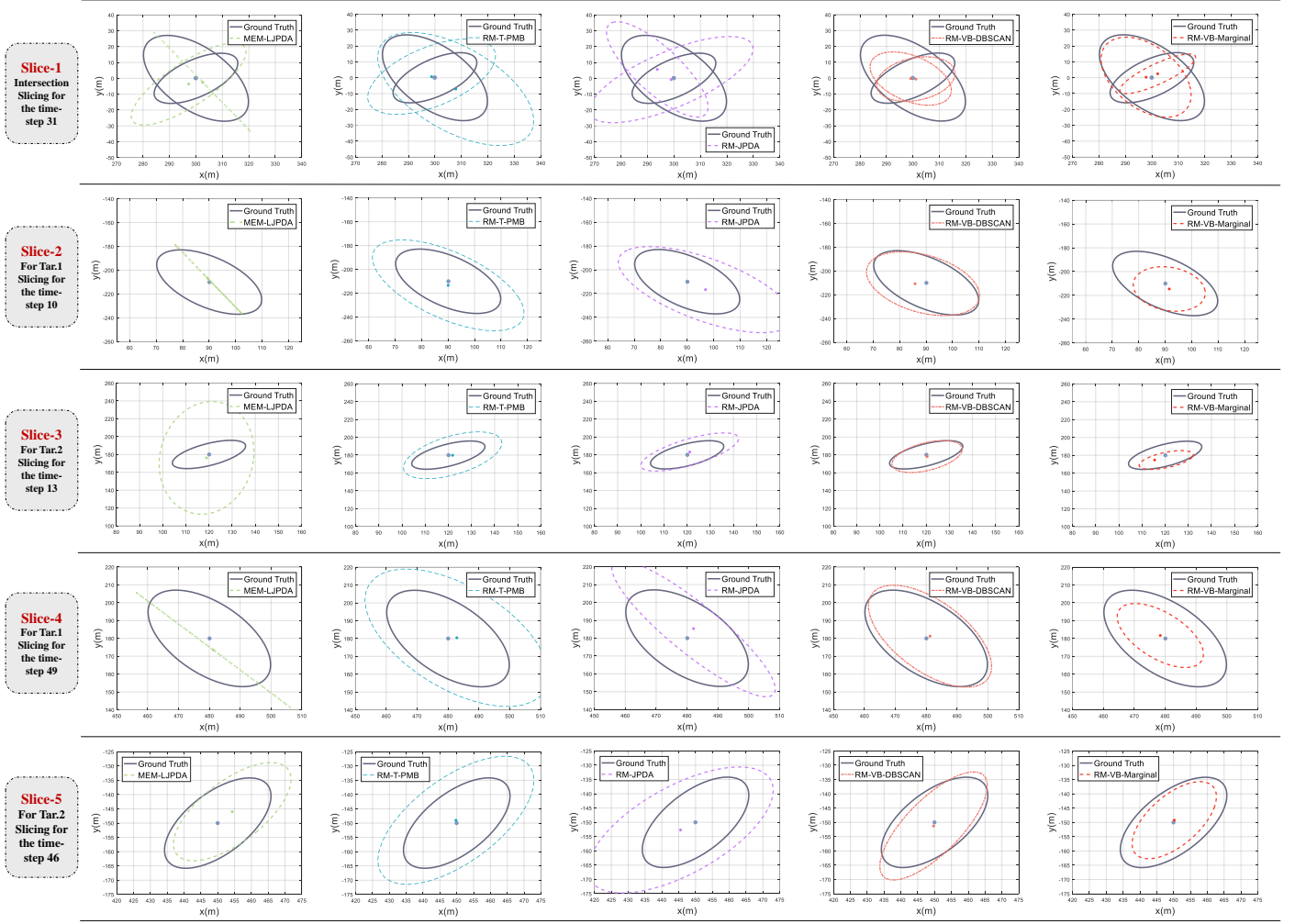


Fig. 7: Enlarged display of the selected slice in Fig. 3. (Showing slice 1, slice 2, slice 3, slice 4 and slice 5 from the top to the bottom of Fig. 7. And the shape estimation of MEM-LJPDA, RM-T-PMB, RM-JPDA, RM-VB-DBSCAN and RM-VB-Marginal are displayed from the left to the right in each row.)

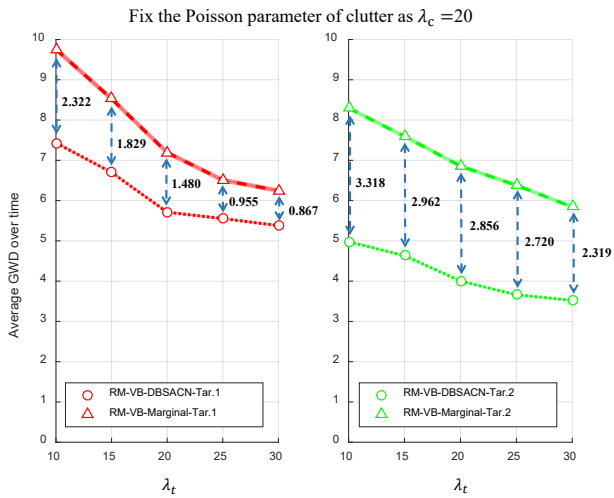


Fig. 8: Average GWD over time with fixed λ_c and variable λ_t of two lightweight schemes.

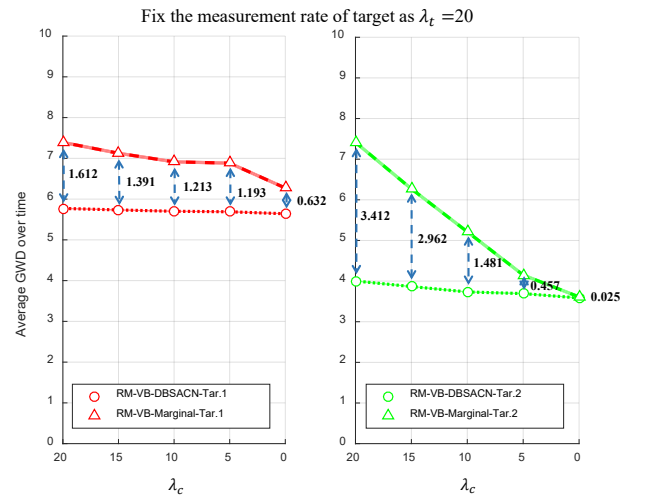


Fig. 9: Average GWD over time with fixed λ_t and variable λ_c of two lightweight schemes.

TABLE IV: Average computational time per MC run of the tracking methods

Tracking Methods	Average computational times per MC run (s)
MEM-LJPDA	6.68
RM-T-PMB	187.27
RM-JPDA	142.121
RM-VB-DBSCAN	150.116
RM-VB-Marginal	11.203



Fig. 10: The trajectories of the targets in real data scenario. In the figure, an initial frame is shown. The color bar shows the time delay of the targets' movement.

D. The Real Data Scenario

In this section, we further illustrate the advantages of the proposed method using real data. The test data are collected on an urban road in Guangdong. The real scenario involves multiple vehicles traveling at an approximately constant speed on the road while using a drone fixed in mid-air to capture images in the surveillance area.

In this scene, we have selected three vehicles of interest for tracking, including a royal blue saloon car (Tar.1), a black saloon car (Tar.2), and a white bus (Tar.3). Their actual trajectories are shown in Fig.10. We use solid lines with gradient colors to indicate the center trajectories. At the beginning of the scene, targets are located at the positions indicated by the corresponding dark blue dots, and then they drive along the paths marked by the lines until surveillance ended at the locations marked by the respective green triangle. The entire scene contains a total of 67 frames, and the time interval of each frame is $T = 0.0625s$.

Throughout the scenario, images captured by the drone are processed for measurement acquisition. We first use an image processing algorithm to separate the objects of interest from the background based on color features. Subsequently, a median filter is employed to reduce the number of clutter⁵. Finally, the target pixels are uniformly sampled to obtain measurements generated by the target surface. This measurement acquisition scheme is consistent with [26]. In addition, since the scene and the size of the target are different from the previous simulation experiments, the parameters of various methods used have been modified as follows:

- For RM-T-PMB, RM-JPDA and our proposed methods, the initial shape parameters are adjusted to be the same and smaller than the actual shape size of the targets, i.e.: $\hat{p}_{0|0}^{(1)} = \hat{p}_{0|0}^{(2)} = \hat{p}_{0|0}^{(3)} = 14$ and $\hat{V}_{0|0}^{(1)} = \hat{V}_{0|0}^{(2)} = \hat{V}_{0|0}^{(3)} = 5$.
- The initial position of each target is set to the initial frame based on their position in the initial frame and plus a Gaussian perturbation with zero mean $\mathcal{N}(0; \text{diag}([5, 5]))$, and the initial kinematic state covariance is reduced by a factor of ten.

Fig.11 shows the estimate of the extent of the target corresponding to frames 10, 20, 30, 40, 50, 60. These slices are chosen to illustrate the performance differences between methods more clearly, and the GWD of the three targets is counted and presented in Fig.12, Fig.13 and Fig.14 respectively.

The conclusions drawn from the simulation experiment in Section 6C are further confirmed by the results shown in the figures. The two traditional RMM-based methods, RM-T-PMB and RM-JPDA, rely on a prior shape parameter setting and cannot accurately estimate the shape of the target. Since MEM-LJPDA does not have parameter modeling for the target measurement rate, its shape estimation converges more slowly and is not accurate enough in the shape estimation of Tar.1 (Fig.12, yellow line). Interestingly, due to less clutter in the scene, RM-VB-Marginal achieved an accuracy that is very close to or even higher than RM-VB-DBSCAN, especially for Tar.1 and Tar.2 (Fig.12 and Fig.13, red line), while ensuring the efficiency of calculation.

VII. CONCLUSION

In this work, we propose a novel variational Bayesian method for multi-target tracking in a cluttered environment. We use the RMM with shape evolution to model the targets and obtain approximate posterior distributions for the targets' joint states based on the VBI. Moreover, two lightweight schemes, based on clustering or marginal association probabilities, are presented as potential solutions to improve the practicality of our method.

The efficacy of the proposed algorithm is validated through both simulation and real data experiments. The experimental results show that, in comparison to the existing multi-target tracking methods, our proposed approach yields superior estimation precision and demonstrates robust adaptability in different measurement environments.

Furthermore, our method exhibits satisfactory scalability and integrability as a consequence of the utilization of the RMM for target modeling. This means that our proposed VBI-based multi-target parameter estimation method can also be integrated into a variety of existing VBI-based single-target state estimation models, such as [26], [34], [43], as a way to expand the application of these models in multi-target tracking.

⁵We retain a small amount of clutter to ensure the authenticity of the scenario. The clutter comes from the background.

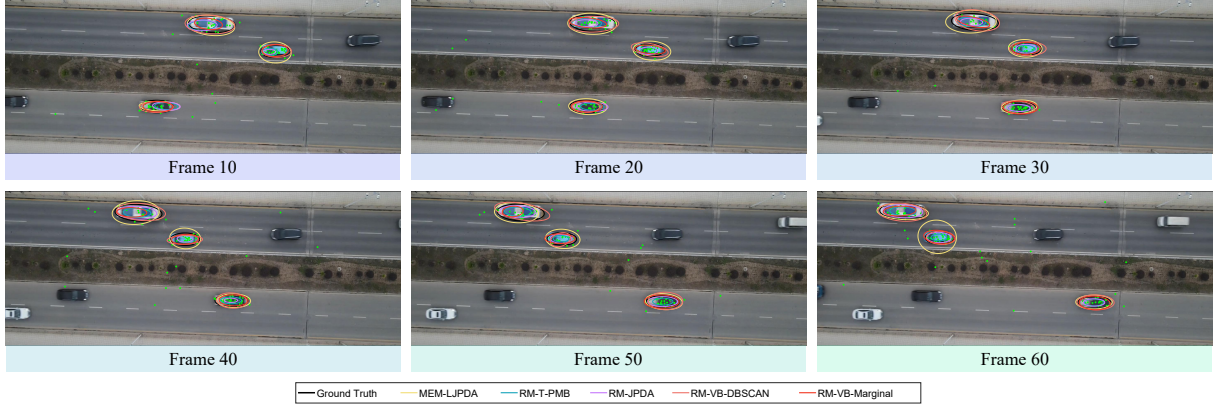


Fig. 11: A representative MC run of the real data experiment. The measurements are represented with green dots.

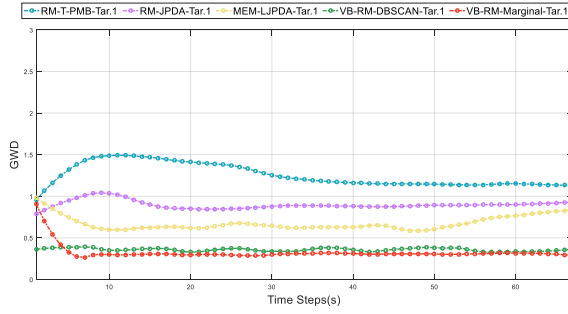


Fig. 12: The GWD of Tar.1 in real data scenario. (Averaged over 100 MC runs)

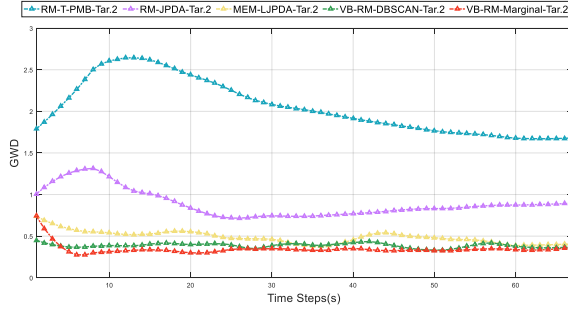


Fig. 13: The GWD of Tar.2 in real data scenario.

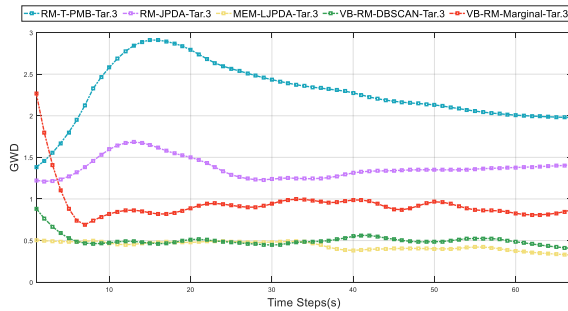


Fig. 14: The GWD of Tar.3 in real data scenario.

REFERENCES

- [1] K. Granström and M. Baum, "A tutorial on multiple extended object tracking," *Techrxiv*, 2022. [Online]. Available: <http://dx.doi.org/10.36227/techrxiv.19115858.v1>
- [2] K. Granström and M. Baum, "Extended object tracking: Introduction, overview and applications," *ArXiv*, vol. abs/1604.00970, 2016. [Online]. Available: <https://api.semanticscholar.org/CorpusID:14452673>
- [3] K. Granström, C. Lundquist, and U. Orguner, "Tracking rectangular and elliptical extended targets using laser measurements," in *Proc. 14th Int. Conf. on Inf. Fusion*, 2011, pp. 1–8.
- [4] J. S. Fowdur, M. Baum, and F. Heymann, "An elliptical principal axes-based model for extended target tracking with marine radar data," in *Proc. 24th Int. Conf. on Inf. Fusion*, 2021, pp. 1–8.
- [5] X. Cao, J. Lan, Y. Liu, and B. Tan, "Tracking of rectangular object using key points with regionally concentrated measurements," *IEEE Trans. Intell. Transp. Syst.*, vol. 25, no. 6, pp. 5312–5327, 2024.
- [6] M. Baum and U. D. Hanebeck, "Extended object tracking with random hypersurface models," *IEEE Trans. Aerosp. Electron. Syst.*, vol. 50, no. 1, pp. 149–159, 2014.
- [7] H. Alqaderi, F. Govaers, and W. Koch, "Symmetric star-convex shape tracking with wishart filter," in *Proc. 24th Int. Conf. on Inf. Fusion*, 2021, pp. 1–8.
- [8] N. Wahlström and E. Özkan, "Extended target tracking using gaussian processes," *IEEE Trans. Signal Process.*, vol. 63, no. 16, pp. 4165–4178, 2015.
- [9] H. Alqaderi, F. Govaers, and W. Koch, "Bayesian wishart filter for random shape tracking," *IEEE Trans. Aerosp. Electron. Syst.*, vol. 58, no. 3, pp. 1941–1952, 2022.
- [10] W. Aftab, R. Hostettler, A. De Freitas, M. Arvaneh, and L. Mihaylova, "Spatio-temporal gaussian process models for extended and group object tracking with irregular shapes," *IEEE Trans. Veh. Technol.*, vol. 68, no. 3, pp. 2137–2151, 2019.
- [11] L. Gao, G. Battistelli, and L. Chisci, "Extended object tracking based on superellipses," in *Proc. 27th Int. Conf. on Inf. Fusion*, 2024, pp. 1–8.
- [12] J. W. Koch, "Bayesian approach to extended object and cluster tracking using random matrices," *IEEE Trans. Aerosp. Electron. Syst.*, vol. 44, no. 3, pp. 1042–1059, 2008.
- [13] M. Wieneke and W. Koch, "A pmht approach for extended objects and object groups," *IEEE Trans. Aerosp. Electron. Syst.*, vol. 48, no. 3, pp. 2349–2370, 2012.
- [14] M. Schuster, J. Reuter, and G. Wanielik, "Probabilistic data association for tracking extended targets under clutter using random matrices," in *Proc. 18th Int. Conf. on Inf. Fusion*, 2015, pp. 961–968.
- [15] K. Granström and U. Orguner, "A phd filter for tracking multiple extended targets using random matrices," *IEEE Trans. Signal Process.*, vol. 60, no. 11, pp. 5657–5671, 2012.
- [16] K. Granström, M. Fatemi, and L. Svensson, "Poisson multi-bernoulli mixture conjugate prior for multiple extended target filtering," *IEEE Trans. Aerosp. Electron. Syst.*, vol. 56, no. 1, pp. 208–225, 2020.
- [17] Y. Xia, "Poisson multi-bernoulli approximations for multiple extended object filtering," *IEEE Trans. Aerosp. Electron. Syst.*, vol. 58, no. 2, pp. 890–906, 2022.

- [18] Y. Xia, K. Granström, L. Svensson, Á. F. García-Fernández, and J. L. Williams, "Extended target poisson multi-bernoulli mixture trackers based on sets of trajectories," in *Proc. 22th Int. Conf. on Inf. Fusion*, 2019, pp. 1–8.
- [19] Y. Xia, Á. F. García-Fernández, F. Meyer, J. L. Williams, K. Granström, and L. Svensson, "Trajectory pmb filters for extended object tracking using belief propagation," *IEEE Trans. Aerosp. Electron. Syst.*, vol. 59, no. 6, pp. 9312–9331, 2023.
- [20] S. Wei, Á. F. García-Fernández, and W. Yi, "The trajectory phd filter for coexisting point and extended target tracking," *IEEE Trans. Aerosp. Electron. Syst.*, vol. 61, no. 3, pp. 5669–5685, 2025.
- [21] J. Lan and X. R. Li, "Tracking of extended object or target group using random matrix: new model and approach," *IEEE Trans. Aerosp. Electron. Syst.*, vol. 52, no. 6, pp. 2973–2989, 2016.
- [22] P. Hoher, S. Wirtensohn, T. Baur, J. Reuter, F. Govaers, and W. Koch, "Extended target tracking with a lidar sensor using random matrices and a virtual measurement model," *IEEE Trans. Signal Process.*, vol. 70, pp. 228–239, 2022.
- [23] S. Yang and M. Baum, "Tracking the orientation and axes lengths of an elliptical extended object," *IEEE Trans. Signal Process.*, vol. 67, no. 18, pp. 4720–4729, 2019.
- [24] S. Steuernagel, K. Thormann, and M. Baum, "Improved extended object tracking with efficient particle-based orientation estimation," in *Proc. 26th Int. Conf. on Inf. Fusion*, 2023, pp. 1–8.
- [25] M. Li, J. Lan, and X. R. Li, "Tracking of elliptical object with unknown but fixed lengths of axes," *IEEE Trans. Aerosp. Electron. Syst.*, vol. 59, no. 5, pp. 6518–6533, 2023.
- [26] B. Tuncer and E. Özkan, "Random matrix based extended target tracking with orientation: A new model and inference," *IEEE Trans. Signal Process.*, vol. 69, pp. 1910–1923, 2021.
- [27] S. Yang, K. Thormann, and M. Baum, "Linear-time joint probabilistic data association for multiple extended object tracking," in *Proc. 10th Sens. Array Multichannel Signal Proces. Workshop*, 2018, pp. 6–10.
- [28] S. Yang, L. M. Wolf, and M. Baum, "Marginal association probabilities for multiple extended objects without enumeration of measurement partitions," in *Proc. 23th Int. Conf. on Inf. Fusion*, 2020, pp. 1–8.
- [29] M. Feldmann, D. Fränken, and W. Koch, "Tracking of extended objects and group targets using random matrices," *IEEE Trans. Signal Process.*, vol. 59, no. 4, pp. 1409–1420, 2011.
- [30] U. Orguner, "A variational measurement update for extended target tracking with random matrices," *IEEE Trans. Signal Process.*, vol. 60, no. 7, pp. 3827–3834, 2012.
- [31] T. Ma, Y. Wang, C. Chen, and K. Cao, "A variational bayesian algorithm for extended target tracking with unknown measurement noise," in *Proc. Chinese Control Conf.*, 2019, pp. 3385–3389.
- [32] J. Lan and X. R. Li, "Extended-object or group-target tracking using random matrix with nonlinear measurements," *IEEE Trans. Signal Process.*, vol. 67, no. 19, pp. 5130–5142, 2019.
- [33] Z. Li, J. Zhang, J. Wang, and Q. Zhou, "Extended object tracking using random matrix with converted measurements," *IET Radar Sonar Navig.*, vol. 14, no. 1, 2020.
- [34] L. Zhang and J. Lan, "Tracking of extended object using random matrix with non-uniformly distributed measurements," *IEEE Trans. Signal Process.*, vol. 69, pp. 3812–3825, 2021.
- [35] R. Gan, Q. Li, and S. J. Godsill, "Variational tracking and redetection for closely-spaced objects in heavy clutter," *IEEE Trans. Aerosp. Electron. Syst.*, pp. 1–24, 2024.
- [36] P. Yun, P. Wu, X. Li, S. He, and K. Wu, "Variational bayesian based adaptive pda filter in scenarios with unknown detection probability and heavy-tailed process noise," *J. Frankl. Inst.*, vol. 358, pp. 4503–4527, 2021.
- [37] X. Yang and Q. Jiao, "Variational approximation for adaptive extended target tracking in clutter with random matrix," *IEEE Trans. Veh. Technol.*, vol. 72, pp. 12 639–12 652, 2023.
- [38] Z. Su, L. Liu, H. Ji, and C. Tian, "A variational bayesian approach for partly resolvable group tracking," *Signal Process.*, vol. 203, p. 108805, 2023.
- [39] B. Tuncer, U. Orguner, and E. Özkan, "Multi-ellipsoidal extended target tracking with variational bayes inference," *IEEE Trans. Signal Process.*, vol. 70, pp. 3921–3934, 2022.
- [40] S. Pei, D. Cheng, C. Chen, and W. Chen, "Multi-ellipsoidal tracking of rotating extended object or target group," in *Proc. 6th Conf. Inf. Commun. Signal Process.*, 2023, pp. 139–143.
- [41] K. Gilholm and D. Salmond, "Spatial distribution model for tracking extended objects," in *IEE. Proc. Radar Sonar. Navig.*, 2005. [Online]. Available: <https://api.semanticscholar.org/CorpusID:123307030>
- [42] Y. Cheng, Y. Cao, T.-S. Yeo, Y. Zhang, and J. Fu, "Variation bayesian interference for multiple extended targets or unresolved group targets tracking," 2025. [Online]. Available: <https://arxiv.org/abs/2407.15226>
- [43] L. Zhang and J. Lan, "Extended object tracking using random matrix with skewness," *IEEE Trans. Signal Process.*, vol. 68, pp. 5107–5121, 2020.
- [44] C. Lundquist, K. Granström, and U. Orguner, "An extended target cphd filter and a gamma gaussian inverse wishart implementation," *IEEE J. Sel. Topics Signal Process.*, vol. 7, no. 3, pp. 472–483, 2013.
- [45] J. S. Fowdur, M. Baum, F. Heymann, and P. Banyas, "An overview of the pakf-jpda approach for elliptical multiple extended target tracking using high-resolution marine radar data," *Remote Sens.*, vol. 15, no. 10, 2023.
- [46] X. Xue, D. Wei, and S. Huang, "A novel tpmbm filter for partly resolvable multitarget tracking," *IEEE Sens. J.*, vol. 24, no. 10, pp. 16 629–16 646, 2024.
- [47] M. Baum, "Linear-time jpda based on many-2-many approximation of marginal association probabilities," *Electron. Lett.*, vol. 51, no. 19, pp. 1526–1528, 1 2015.
- [48] D. Deng, "DbSCAN clustering algorithm based on density," in *Proc. 7th Int. Forum Electr. Eng. Autom.*, 2020, pp. 949–953.
- [49] S. Yang, M. Baum, and K. Granström, "Metrics for performance evaluation of elliptic extended object tracking methods," in *IEEE Int. Conf. Multisensor Fusion Integr. Intell. Syst.*, 2016, pp. 523–528.